To the graduate council:

I am submitting herewith a thesis written by Pierre J Morel entitled "EFFECTS OF TEMPERATURE AND STRAIN RATE ON THE SCRATCH RESISTANCE OF POLY-METHYLMETHACRYLATE." I have examined the final paper copy of this thesis for form and content and recommend that it be accepted in partial fulfillment of the requirements for the degree of Master of Science, with a major in Material Science and Engineering.

George R. Pharr

Dr George Pharr, Major Professor

We have read this thesis and
Recommend its acceptance:

Ken Ret

Raymond A. Buchanan

Acceptance for the Council:

Vice Provost and Dean of
Graduate Studies

EFFECTS OF TEMPERATURE AND STRAIN RATE ON THE SCRATCH RESISTANCE OF POLY-METHYLMETHACRYLATE

Thesis

Presented for the

Master of Science

Degree

The University of Tennessee, Knoxville

Pierre Jean MOREL

May 2002

Thesis
2002
.M67

DEDICATION

This thesis is dedicated to my parents, Patrick and Therese Morel, great models, to Vanessa, for her growing role in my life, and to my brothers and sister, Benoit, Myriam and Paul, for their love and support to reach higher and achieve my goals.

ACKNOWLEDGMENTS

First, I want to thank God for giving me the intellectual and physical ability to achieve this work.

I would also like to thank my adviser, Dr. George Pharr of the University of Tennessee, for welcoming me into his research group, for his support and his well-directed advice.

I would like to thank also Dr. Vincent Jardret, from MTS Nano Instruments at Oak Ridge. He has provided me with a great deal of knowledge concerning the testing apparatus used in this work and his previous work on the subject. Without his help, my entire stay in the USA would have been much more difficult.

This work would not have been done without the support of the "Nano Folks". Here, I want to thank Mike, Warren, Barry, Jenny, Erik, Kermit for their scientific and technical help, Greg and John for their "stress reliever time" at the range, and Donna and Valarie, for their joyful nature and daily help.

Finally I want to thank my parents, siblings and Vanessa for supporting me in all my decisions and letting me go far from home.

I gratefully acknowledge support for this research from MTS Nano Instruments in Oak Ridge.

ABSTRACT

The scratch resistance of polymers has been the subject of numerous studies that have led to the characterization of plastic and fracture phenomena during scratching. Viscoelastic and viscoplastic behavior during scratching have been related to dynamic mechanical properties that can be measured via dynamic nano-indentation testing. Yet, an understanding of the origin of the fracture phenomena in a polymer during scratching remains approximate. Parameters like tip geometry and size, scratch velocity and loading rate, and applied strain and strain rates, have been considered critical parameters for the fracture process, but no correlation has been clearly established.

The goal of this work was to evaluate scratch resistance parameters as a function of temperature and strain rate, and compare them to dynamic mechanical properties obtained from nano-indentation tests over a range of temperature for poly-methylmethacrylate (PMMA). Fracture in scratch testing is modeled as resulting from tensile stresses behind the scratch tip. A new scratch fracture parameter is introduced that is related only to material properties and not to the scratch tip geometry. This study brings a new understanding to the origin of fracture mechanisms during scratch testing, and to the influences of indentation strain on the fracture strength of PMMA.

TABLE OF CONTENTS

CHAPTER 1: INTRODUCTION 1

1.1 REASONS FOR DEVELOPING THE SCRATCH TEST 3

1.1.1 INDUSTRY 3

1.1.2 LINKING WEAR PROBLEMS TO MECHANICAL PROPERTIES 5

1.2 IMPORTANCE OF SCRATCH TESTING 9

CHAPTER 2: SCRATCH TESTING 13

2.1 IMPORTANT PARAMETERS IN SCRATCH TESTING 13

2.1.1 SCRATCH TIP GEOMETRY 13

2.1.2 ATTACK ANGLE 16

2.1.3 SPHERE RADIUS 19

2.1.4 SCRATCH SPEED 22

2.2 DEFORMATION AND DAMAGE DURING SCRATCH TESTING 22

2.2.1 ELASTIC / PLASTIC DEFORMATION 23

2.2.2 FRACTURE 30

CHAPTER 3: INSTRUMENTS / EXPERIMENTS 34

3.1 INSTRUMENTATION 34

3.1.1 OVERVIEW OF THE NANO INDENTER XP® 34

3.1.2 DYNAMIC PROPERTY MEASUREMENT 36

3.1.3 TEMPERATURE CAPABILITY 39

3.1.4 SCRATCH TEST EXPERIMENTS 39

3.1.4.1 Scratch testing procedure 39

3.1.4.2 Relation between scratch and indentation measurements 40

3.1.4.3 Lateral force measurement 43

3.2 INDENTER GEOMETRY CHARACTERIZATION 43

3.3 CRITICAL LOAD AND FRACTURE ANALYSIS 48

CHAPTER 4: EXPERIMENTAL RESULTS AND DISCUSSION 53

4.1 INDENTATION RESULTS AS A FUNCTION OF TEMPERATURE 53

4.2 SCRATCH RESULTS AS A FUNCTION OF TEMPERATURE 54

4.2.1 RELATION WITH MECHANICAL PROPERTIES 57

4.2.2 DEPENDENCE OF THE CRITICAL LOAD ON TEMPERATURE 62

4.2.3 COMPARISON OF CRITICAL LOAD TO TENSILE BEHAVIOR 66

4.2.4 HYPOTHESIS FOR THE ORIGIN OF FRACTURE DURING SCRATCH TESTING...71

4.3 INFLUENCE OF INDENTER SHAPE ON DEFORMATION BEHAVIOR AND STRAIN RATE 73

4.3.1 GEOMETRICAL CONSIDERATIONS 73

4.3.2 STRAIN RATE.....75

4.3.2.1 Results for a 90˚ angle cone with a 2 µm tip radius 77

4.3.2.2 Results for a 60˚ cone with a 4 µm tip radius.....80

4.3.3 INFLUENCES OF DEFORMATION ON FRACTURE DURING SCRATCHING.....83

4.3.4 USE OF THE RESULTS IN SCRATCH ANALYSIS.....98

4.3.4.1 Unknown Material.....100

4.3.4.2 Material with a known scratch behavior 103

CHAPTER 5: CONCLUSIONS 105

CHAPTER 6: SUGGESTIONS FOR FUTURE RESEARCH WORK.....107

FIGURES

Figure 1: scratch testing as a bridge between empirical observation and mechanical properties of a material. 7

Figure 2: Influences of mechanical properties on scratch behavior (from C.Xiang, H.J Sue, J.Chu, B. Coleman [16]) 8

Figure 3: Single asperity in contact with a surface [MTS systems] 10

Figure 4: The scratch test can be seen as a test which decreases the complexity of the abrasive contact from a real multiple asperities to single asperity contact 11

Figure 5: Two different ways of scratching a surface with a pyramidal tip: edge or face forward. 15

Figure 6: Definition of attack angle 17

Figure 7: Effect of variation of the attack angle on scratch processes 18

Figure 8: Attack angles for Berkovich and a cube corner scratch tips (face first orientation) 20

Figure 9: Variable attack angle for spherical scratch tip. 21

Figure 10: Model for the partition of scratch deformation in two terms: elastic and plastic plowing (according to Gauthier [23]) 24

Figure 11: Cross sectional profile PMMA after a scratch was made at 100°C and 30mN load. 25

Figure 12: Contact area definition for a spherical scratch tip in the case of a fully developed plastic contact 28

Figure 13: Contact area for the case of elastic-plastic contact 29

Figure 14: Different types of fracture during scratch testing of polymers. 31

Figure 15: Delamination of a polymer film on a glass substrate 32

Figure 16: Schematic diagram of a Nano Indenter® XP with scratch testing capability 35

Figure 17: The four main parts of the scratch testing procedure 41

Figure 18: Forces during scratch testing 44

Figure 19: Characterization of the conical geometry of the indenter/scratch tip by a half included angle, α, and a tip radius, R. 45

Figure 20: Relationship between the height and width of the scratch tip 47

Figure 21: Indications of fracture on the post scratch profile and the scratch segment data 49

Figure 22:Fracture obtained with a 60° cone on a compound polymer coating (unknown composition)..... 51

Figure 23: Fracture of PMMA at 80°C, obtained with a 90° cone and a 100mN load. 51

Figure 24: Fracture obtained with a cube corner on automotive paint. 52

Figure 25: Fracture and delamination of a polymer compound (unknown composition) on a glass substrate due to scratching with a 60° cone. 52

Figure 26: Effect of temperature on hardness and storage modulus for PMMA55

Figure 27: Effect of temperature on loss modulus and tan δ for PMMA..... 56

Figure 28: Dependence of indentation hardness and scratch hardness on temperature 58

Figure 29: Dependence of pile-up height and the ratio E'/H, on temperature... 60

Figure 30: Cross sectional profiles at different scratch speed 61

Figure 31: Dependence of critical load on temperature for scratch testing of PMMA..... 63

Figure 32: Observation of the fracture during scratch testing at different temperatures..... 64

Figure 33: Optical micrograph of the end of the scratch track demonstrating that fracture occurs behind the contact. 65

Figure 34: Stress/strain curves for PMMA in compression tests [38].....67

Figure 35: Stress/strain curves for PMMA in tensile tests [38].....68

Figure 36: Temperature dependence of σ_Y (yield stress) and σ_B (stress required to cause brittle fracture) for PMMA [38]. Note that the strain rate has a strong influence on the position of the transition temperature (shown in Figure 39).....70

Figure 37: Explanation for the origin of fracture and stresses around the scratch tip.....72

Figure 38: Parameters for description of the scratch tip geometry.....74

Figure 39: Effect of an increase in the strain rate on σ_B and σ_Y at temperature. The curves are shifted to the right and higher [38].....76

Figure 40: Critical load vs. scratch strain rate for a 90˚ cone with a 2µm radius.....79

Figure 41: Critical load as function of temperature and effects of strain rate on the critical load at room temperature for scratch tests in PMMA using a 90˚ cone.....81

Figure 42: Critical load vs. scratch strain rate for 60˚ cone with a 4µm tip radius.....82

Figure 43: Equivalent strain generated by a 90˚ cone with a tip radius of 2µm.86

Figure 44: Equivalent strain vs. contact radius for the two different scratch tips: a 60˚cone with a 4µm radius and a 90˚ cone with a 2µm radius.....87

Figure 45: Contact radii at fracture for different scratch speeds demonstrating the equivalent strain at fracture for the 90˚ cone 89

Figure 46: Contact radii at fracture for different scratch speeds demonstrating the equivalent strain at fracture for the 60˚ cone 90

Figure 47: Equivalent strain vs. critical strain rate for the two scratch tips and their respective fits 95

Figure 48: Critical load vs. scratch strain rate defining the limits of the domain of fracture 97

Figure 49: Effect of an increase in the strain rate on the fracture process for the two different scratch tips 99

Figure 50: Process for determining the critical properties of an unknown material by scratch testing 101

Figure 51: Dependence of scratch hardness on strain rate for PMMA 102

Figure 52: Process for predicting the point of fracture by scratching test on a known material 104

SYMBOLS

a: Residual scratch width

$\mathbf{A_n}$: Projected contact area during scratch experiment

$\mathbf{F_N}$: Normal force on the scratch tip

$\mathbf{F_T}$: Tangential force on the face of the scratch tip

τ: Friction stress on the face of the scratch tip

δ: Angle, relative to the horizontal, of the friction stresses

α: Angle between the face of the scratch tip and the vertical direction

p: residual depth of the groove

$\mathbf{h_b}$: height of the pile-up pads

S: Dynamic stiffness of contact

D: Contact damping

ω: Angular frequency of oscillation

A: Area of contact in indentation

H: Indentation hardness

P: Load applied on the sample

$\mathbf{H_s}$: Scratch hardness

E': Storage modulus

E'': Loss modulus

tan δ: Tangent delta

R: Radius of the spherical part of tip

$\mathbf{h_{sp}}$: Height of the spherical part on the indenter/scratch tip

α: Half angle of the conical indenter/scratch tip

$\mathbf{V_{tip}}$: scratch speed

$\boldsymbol{\sigma_y}$: Yield stress

$\boldsymbol{\sigma_B}$: Ultimate tensile stress

$\mathbf{r_c}$: Contact radius

$\dot{\varepsilon}_i$: Indentation strain rate

$\dot{\varepsilon}_S$: Scratch strain rate

$\mathbf{r_{hsp}}$: Contact radius at the end of the spherical part

$\boldsymbol{\varepsilon_c}$: Deformation due to the cone

$\boldsymbol{\varepsilon_s}$: Deformation due to the sphere

d: depth of penetration of the scratch tip

CHAPTER 1: INTRODUCTION

Perhaps the oldest way for measuring the hardness of a material is based on a scratch test. Mineralogists first developed this kind of testing to evaluate the hardness of stones. The hardness scale that resulted from this work was based on the ability of one material to scratch or to be scratched by another [1]. An article by Blau [2] explains that more recently, the scratch test has found new applications in efforts directed towards understanding the fundamental mechanisms of wear and adhesion [3]. Scratching, abrasion, and wear are all factors that diminish the properties of a surface [4].

There has also been in recent years a significant increase in the number of studies of the mechanical properties of polymers [5]. The combination of their low cost and the fact that they are easy to form and mold has generated an increasing use of polymer materials as surface coatings. Nevertheless, their lifetime is often limited by their poor mechanical properties. For example, automotive paints are subject to numerous forms of degradation. Among them, scratching and abrasion are primarily responsible for the degradation of appearance and loss of optical performance of these materials [6,7,8,9].

As a simplification of complex abrasion processes, the scratch test has been used with success to identify the main parameters responsible for the wear resistance of materials [10]. However, how the properties measured during a scratch test relate to the mechanical properties of a material is still not fully understood. Results from scratch testing have often been used to rank materials but have rarely been linked to the fundamental mechanical properties of the material.

This work will present, first, the motivation for such a study. Specifically, industry is more and more concerned about the behavior of polymer products. Even though their industrial use is very common, polymer behavior is still not fully understood.

It is then necessary to understand basics models used to study scratch behavior and progress made in understanding scratch testing. Different parameters that are important either in the way the scratch test is conducted, or in the analysis of the results from experiments, are discussed.

New experimental results are then presented that relate properties measured in scratch test at temperature to mechanical properties measured by indentation for poly-methylmethacrylate (PMMA). An explanation for the origin of fracture in scratch testing is proposed that is related to the tensile stresses in the

material in the region behind the scratch tip. Finally, an examination of the influences of strain and strain rate in a scratch experiment leads to a new fracture parameter that is only dependent on the material and independent of the tip geometry.

1.1 Reasons for developing the scratch test

In addition to the empirical way it is used to estimate hardness, the scratch test is used more and more frequently to study the mechanisms of degradation of a surface. In this regard, the scratch technique has been used to solve several important industrial problems.

1.1.1 Industry

Due to the importance of damage caused by wear of moving parts, industry has invested heavily in the study of tribological properties. Wear can have various detrimental consequences like the loss of function of a part in a mechanism, or the loss of the esthetic appearance of a device. In order to have a better understanding of the importance of the problem it is constructive to consider an example.

For a long time now, car buyers have required both beauty and performance, and that both these qualities be durable [11]. As automotive paint finishes have become more and more mirror-like, defects in paints have become more visible to the customer, resulting in increasing complaints. Most new cars now have a paint composed of a basecoat/clearcoat coating system. The basecoat provides the color and the clearcoat gives the high gloss attributes. Scratching and marring, which first affect the clearcoat, can be caused during shipping from the factory, or after purchase due to car washes and normal day-to-day wear and tear. Scratching not only causes of the loss of appearance, but also after a certain time, the loss in the chemical resistance of the paint and decrease in the protection of the basecoat.

Large automotive paint manufacturers, like Bayer [6,7,11], or DuPont [9,5], want to improve the quality of their automotive paints. One of the problems they have is the automatic carwash, which is a normal recurrent activity. The brushes used in the automatic carwash often scratch paint, and diminish the visual appearance of the car.

The first step towards reproducing these wear conditions was to submit a sample of paint to the brushes in rotation [6, 7, 11]. This gave the number of scratches and the wear rate of the paint as a function of time. In addition, the scratch resistance was related to the hardness of the coating, which allowed

them to rank the different paints. However, they also wanted to improve the chemical composition of their paints. In order to do so, they had to know which component in the polymer composition could improve the properties and scratch resistance of the paint. What was needed was a way of estimating not only qualitatively but also quantitatively, the scratch resistance and the mechanical properties of the paints. The scratch test was adopted by many paint manufacturers for this purpose [9]. More and more car manufacturers like Ford and General Motors [12, 13, 14, 15], have begun to use micro and nano scratch tests in order to relate the scratch resistance of their automotive paints to their the mechanical properties and performance.

1.1.2 Linking wear problems to mechanical properties

Wear problems in materials are notoriously difficult to quantify. During the design of a product, the main information available to designers are material properties and the previous observations. On the one hand, observations are made "in the field" with the surface submitted to real abrasion and wear conditions. On the other hand, the designer has to choose a material for a certain application, and his decision is based on the intrinsic characteristics of the material.

It is then important to develop tools that can bridge these two domains. The scratch test can be seen as a important step in trying to relate mechanical properties and tribological properties of the material, as shown in Figure 1. Other important information can be obtained in indentation and tensile tests and in wear tests (pin on disc). The scratch test is included in this general effort as a way to find a relationship between what is sought in design and the real performance of parts subject to wear. Xiang, Sue, et al. [16] have investigated how mechanical properties can affect scratch visibility on polymers. They have explained that a scratch is noticed by a human eye for two main reasons: the groove due to a plastic flow of the material, and the fracture of the material. They then tried to find the mechanical properties that would influence the flow and the fracture of the material. Their results, shown as a flow chart in Figure 2, present the influence of the mechanical properties on these two phenomena.

The aim of the present work is to use the well known, ductile-to-brittle-transition in the tensile deformation of polymeric materials over a defined range of temperature and strain rate in order to achieve a better understanding of the influence of ductile and brittle behavior on scratching.

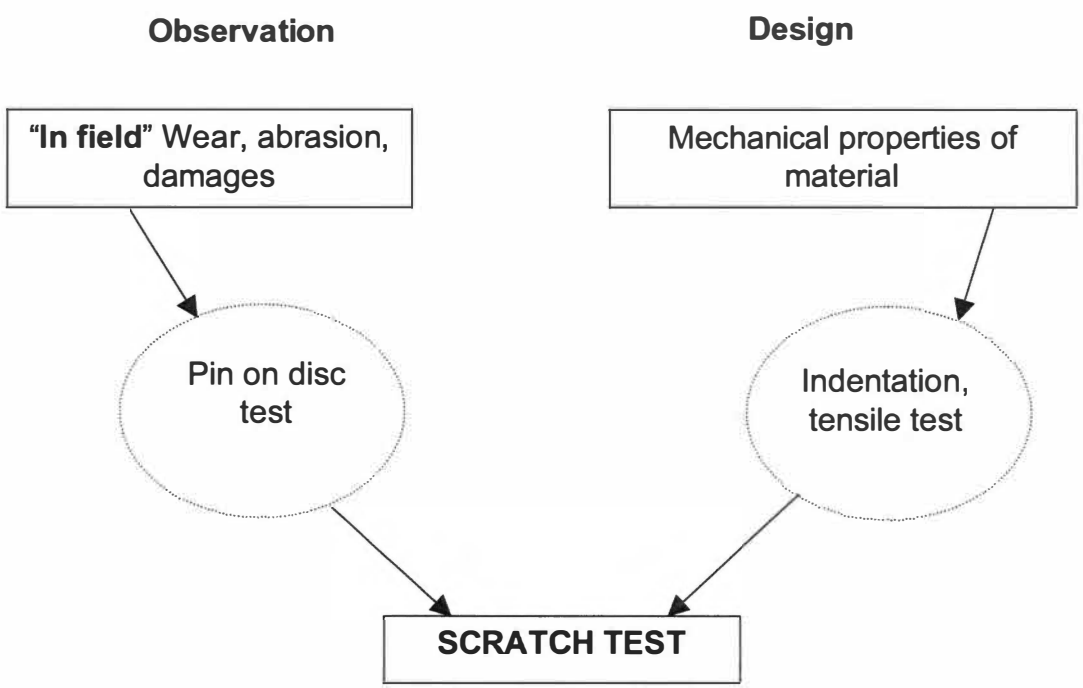


Figure 1: scratch testing as a bridge between empirical observation and mechanical properties of a material.

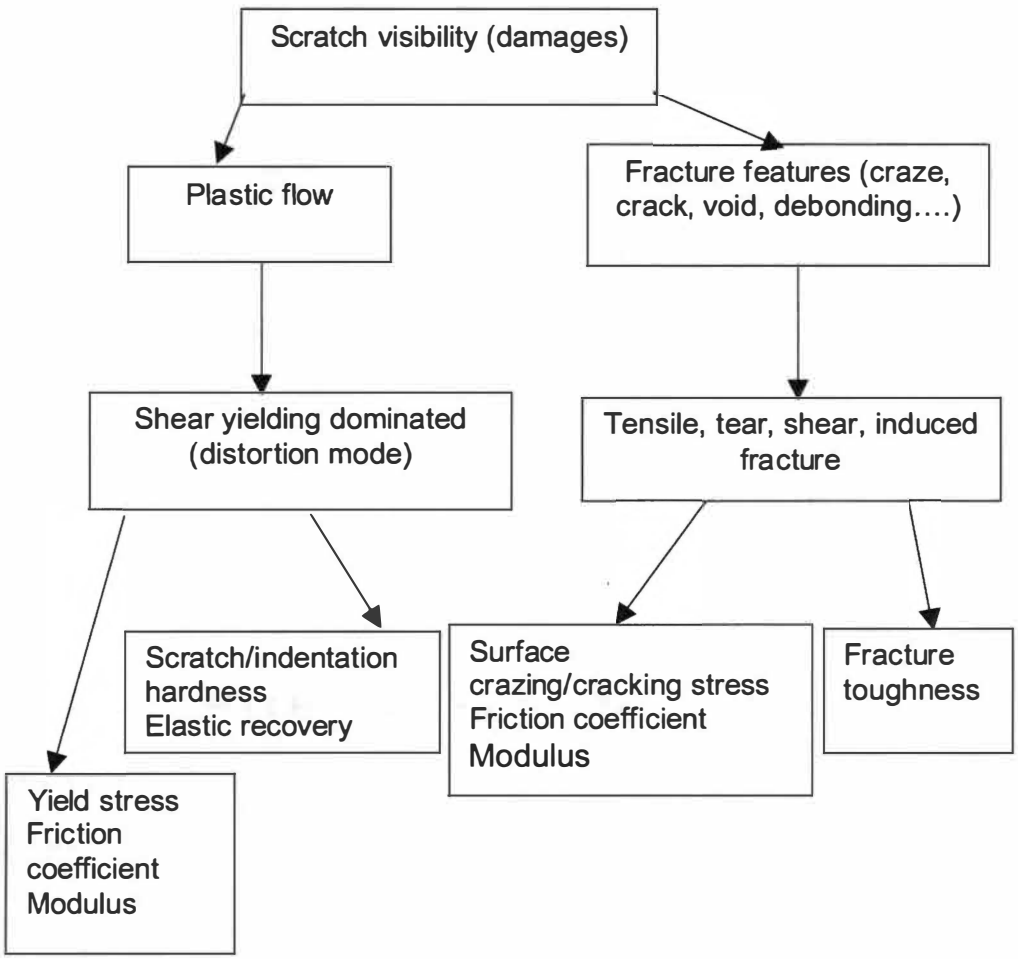


Figure 2: Influences of mechanical properties on scratch behavior (from C.Xiang, H.J Sue, J.Chu, B. Coleman [16])

1.2 Importance of scratch testing

Scratching can be defined as the deformation and damage caused by the motion of a sharp object, the "**scratch tip**", in contact with a surface.

The scratch can be used as a model for two types of real situations. The first is a single scratch on a surface. This would be the equivalent of a sand grain scratching an automotive paint, a key scratching a car (Figure 3), or a dust scratching the lens of a camera. In this case, the scratch tip represents only one asperity, which slides on the surface with a load applied to it, creating the scratch.

The second situation that can be modeled by scratch testing is for complex wear problems. This would be the case of a brush cleaning the car, in which there are multiple points of contacts and asperities. For this situation, the scratch tip represents a simplification of the complex abrasive situation. Figure 4 shows how the scratch test represents only what is happening for one asperity instead of the complex effect of all the asperities involved in the real contact. Ideally, one can generalize the results of the scratch test to understand the larger complex abrasion problem.



Figure 3: Single asperity in contact with a surface [MTS systems]

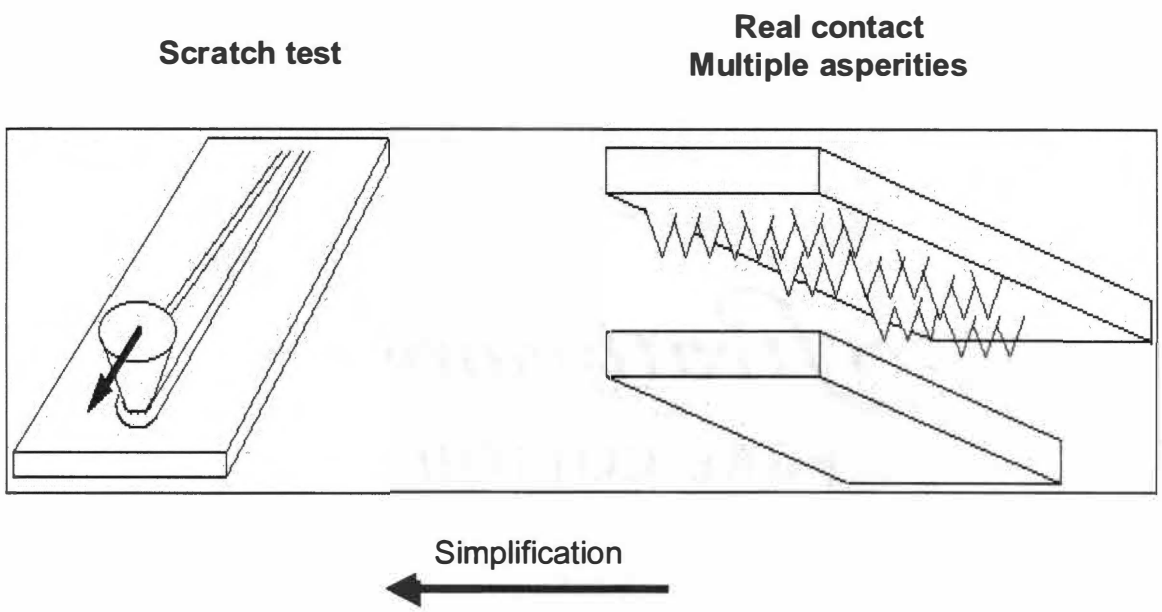


Figure 4: The scratch test can be seen as a test which decreases the complexity of the abrasive contact from a real multiple asperities to single asperity contact.

In both situations, the scratch process generates deformation on the surface, which can be classified as elastic, plastic, fracture and delamination.

CHAPTER 2: SCRATCH TESTING

In this chapter, we will consider a scratch tip sliding on a surface with a normal load applied to it, and examine the important parameters derived from such a test; special attention will be paid to the deformation and damage produced during scratching.

In order to understand the scratch test, several parameters must first be defined. Many of these parameters are related to the geometry of the contact and the kinetics of the scratch tip on the surface

2.1 Important parameters in scratch testing

2.1.1 Scratch tip geometry

The geometry of the scratch tip used to generate the scratch is of primary importance in the scratch process. The scratch tip can have many different shapes. These shapes reproduce approximately all the possible geometries

that an asperity can have in a real contact. A non-exhaustive list of the shapes would be:

- ✓ Conical
- ✓ Pyramidal: Berkovich, Vickers, cube corner....
- ✓ Spherical
- ✓ Flat punch

The geometry of the scratch tip has an important effect on the type of deformation and stresses induced in the material. For example, the edges of the pyramidal shapes generate a concentration of stress at these geometrical singularities. Thus, the Berkovich tip will generate a stress field quite different than a sphere, due to the presence of the edges, which act like a knife. The flow of the material in front of the scratch tip is different for a cone and a pyramid. For the cone, the material does not meet a discontinuity in the surface geometry, whereas for the pyramid, material flows along one surface until it finds an edge where the characteristics of the flow change. Furthermore, for the pyramidal shape, the scratch behavior is different when the scratch tip moves in an edge or face forward, as shown in Figure 5. In these two extreme cases, the deformation is different due to a different stress fields [17, 18]. In a brittle or semi brittle material, the presence of edges has a strong influence on the fracture because of the stress concentrations they generate [19].

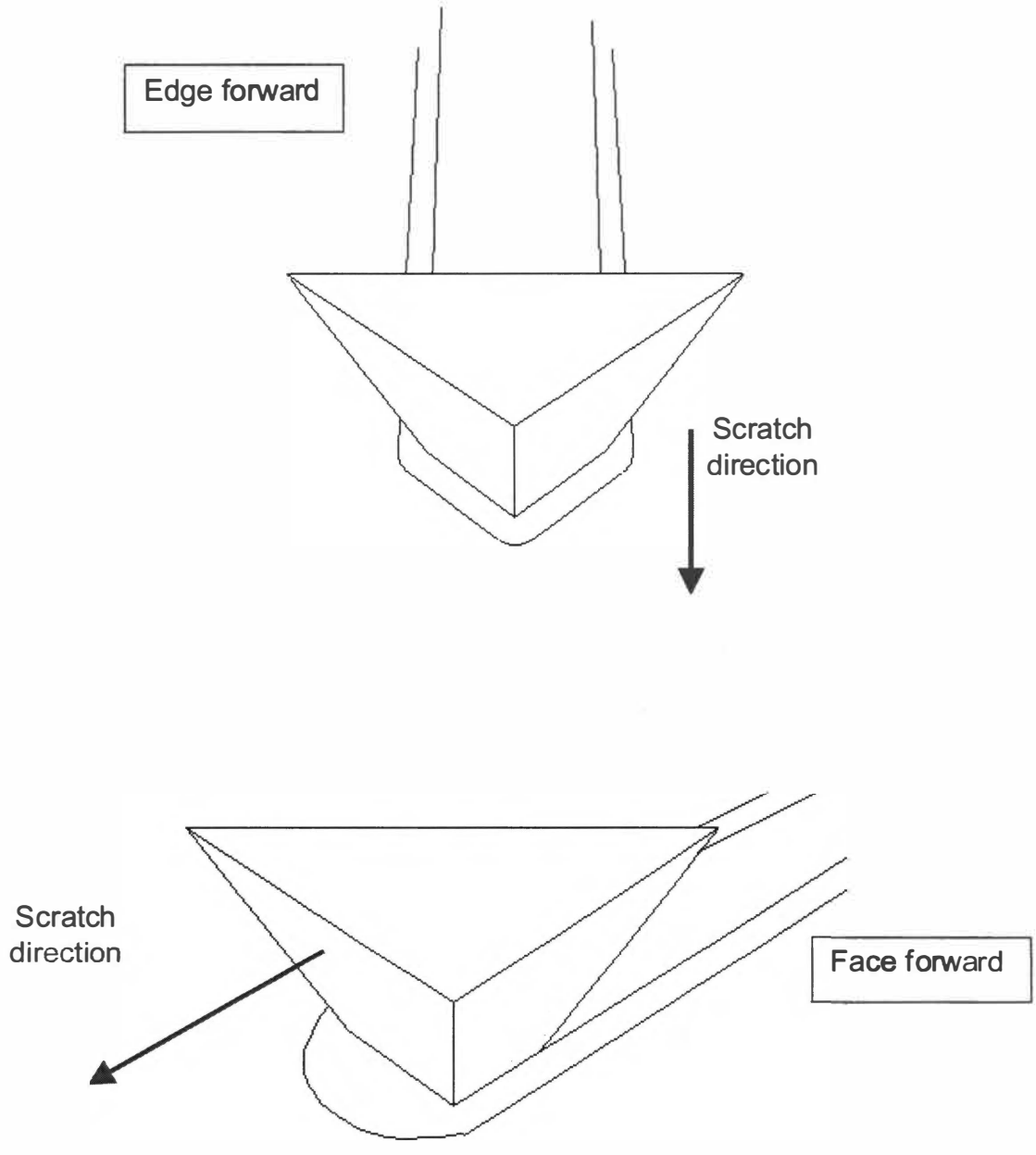


Figure 5: Two different ways of scratching a surface with a pyramidal tip: edge or face forward.

2.1.2 Attack angle

The attack angle is defined as the angle between the surface scratched and the scratch tip surface (Figure 6). The attack angle, like the scratch tip shape, has an important influence on the type of deformation and damage caused to the surface. The smaller the attack angle, the less severe the abrasive contact. In order to understand this clearly, the simple example of a knife and butter can help.

If one takes a knife and slides it on the surface of the butter at different angles (Figure 7), different results will be obtained. If the attack angle between the blade and the butter is small, the knife will slide on the butter without too much effect. Increasing the attack angle makes the blade penetrate into the butter, thereby pushing a volume of butter in front of the knife. If the angle becomes too large, the deformation changes into a cutting behavior. In this case, the butter is shaved as a chip of material is formed and slides up on the scratch tip surface.

Elastic, ductile and brittle behaviors during scratching have been studied by Briscoe [20, 21], and Atkins [22]. Cutting behavior is triggered by a critical

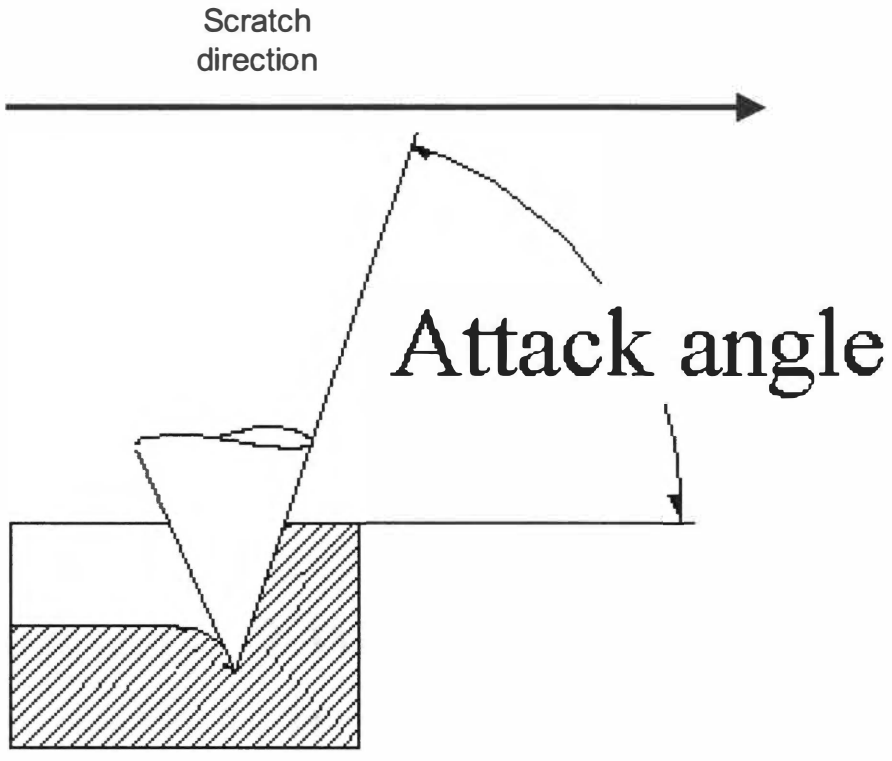


Figure 6: Definition of attack angle

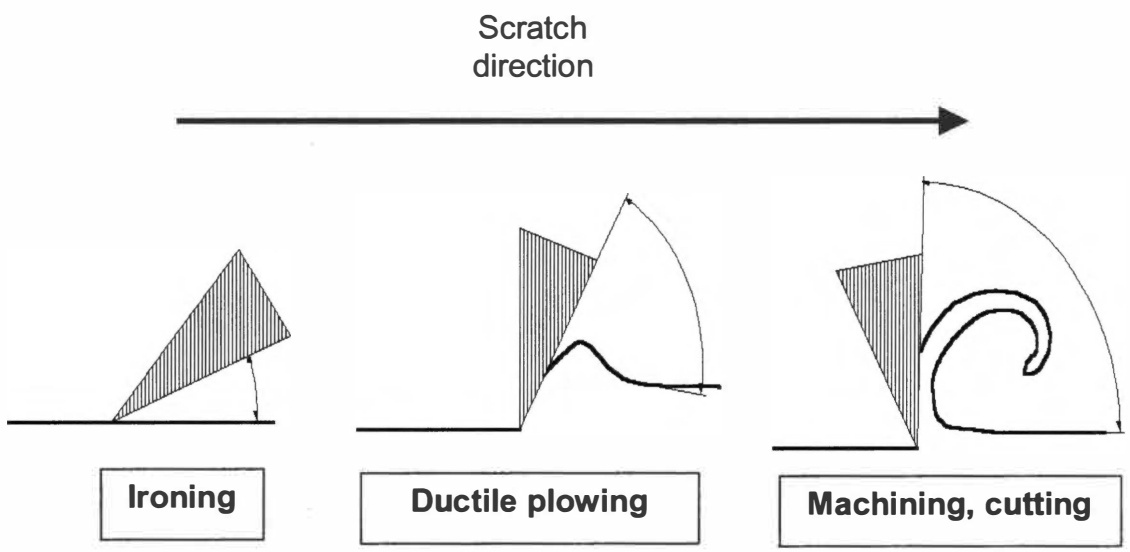


Figure 7: Effect of variation of the attack angle on scratch processes

value of the attack angle. This behavior is important in understanding metal cutting during machining. In this work, the angle will be kept smaller than the cutting angle. In the case of pyramidal shaped tips, the scratch tip shape determines the attack angle (Figure 8).

The attack angle is one important aspect of the geometry of the contact between the scratch tip and the surface. The attack angle determines the severity of the deformation, and thereby the damage that results from sliding contact.

2.1.3 Sphere radius

In the case of a sphere sliding on a surface, the attack angle is not constant if the load is increased as the scratch is made. As shown in Figure 9, the attack angle is very small at the point of first contact between the sphere and the surface, and then, as the sphere penetrates into the surface, the attack angle increases. For extreme cases, the attack angle is equal to zero initially, and reaches 90 degrees when half of the sphere penetrates into the material. The fact that the attack angle varies also has a strong influence on the strain induced in the material.

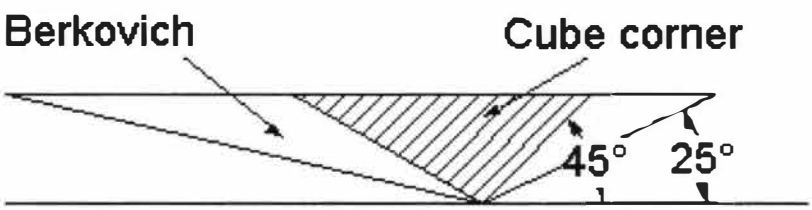


Figure 8: Attack angles for Berkovich and a cube corner scratch tips (face first orientation)

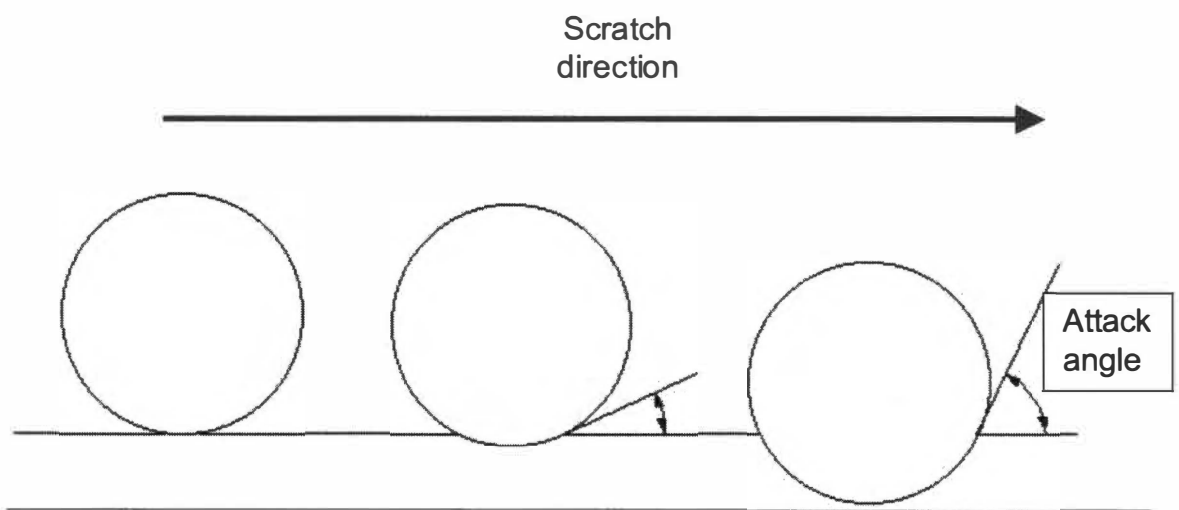


Figure 9: Variable attack angle for spherical scratch tip.

2.1.4 Scratch speed

As a scratch tip moves on the surface, the parameters controlling its motion also have an influence on the scratch behavior. The most important parameter is the speed of the scratch tip on the surface. The speed of the scratch tip controls the velocity of material flow around the scratch tip and the level of the local stresses for a strain rate sensitive material. This speed is directly related to the strain rate induced in the material. Briscoe, Gauthier, Lafaye, and Schirrer [20, 23, 24, 25], have examined the influence of scratch speed on deformation. For conical and pyramidal indenters, an increase in the scratch speed generates proportionally an increase in the strain rate. In the case of polymers and time-temperature dependent materials, a high scratch speed that induces a high strain rate will dramatically change the material response. This emphasizes the importance of the scratch speed in the study of polymers.

2.2 Deformation and damage during scratch testing

A scratch experiment can generate many kinds of deterioration behavior and damage, which require different parameters to describe. The scratch deterioration behaviors are often categorized as follows:

- ✓ Elastic-plastic behavior
    - o Visco-elastic
    - o Visco-plastic
    - o Fracture behavior

2.2.1 Elastic / Plastic deformation

Gauthier and Schirrer [23] have used a model for scratching in which the deformation can be split in two terms (Figure 10): the elastic and plastic plowing terms. Elastic deformation is reversible and is recovered behind the scratch tip. Plastic plowing is permanent deformation that can be observed afterwards by making a cross sectional profile of the scratch.

Plastic deformation produces a groove that is flanked by two lateral pile-ups. Plastically deformed scratch tracks can be described by the following parameters shown schematically in Figure 11:

Scratch width **a** : The distance between the peaks of the pile-up on each side of the groove.

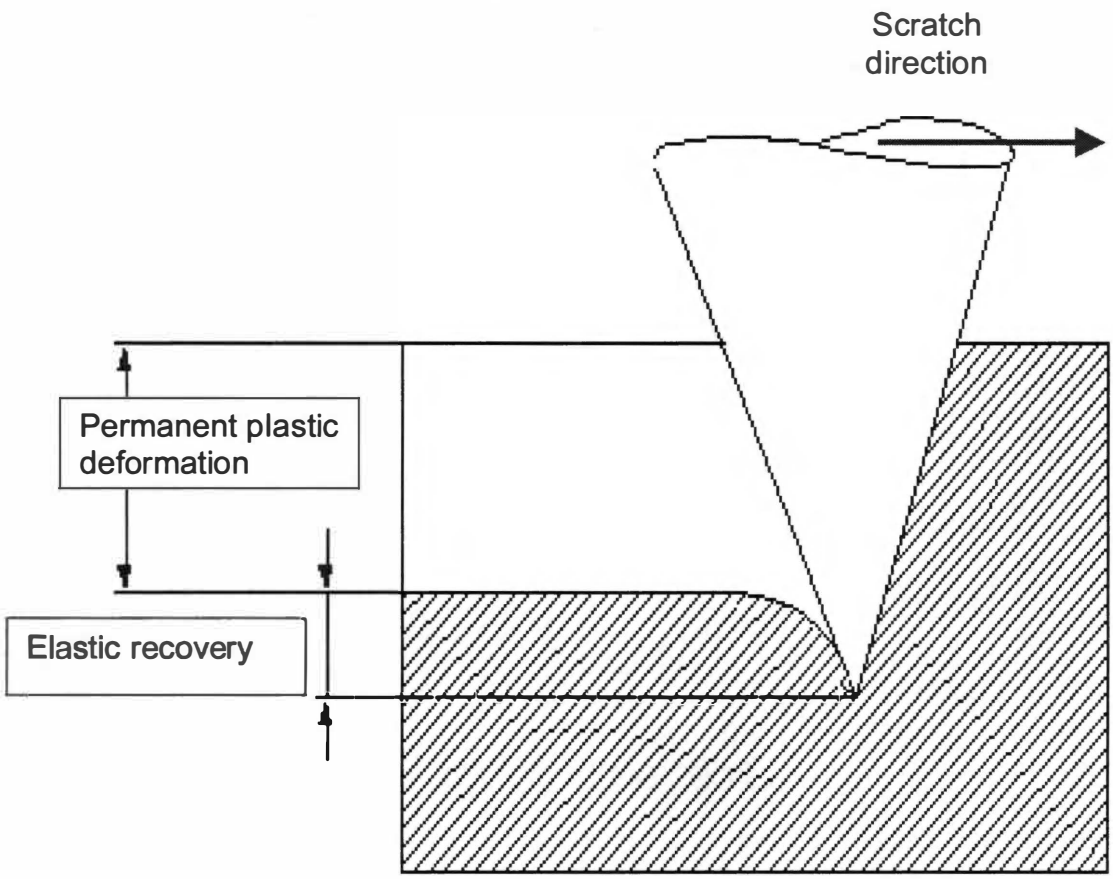


Figure 10: Model for the partition of scratch deformation in two terms: elastic and plastic plowing (according to Gauthier [23])

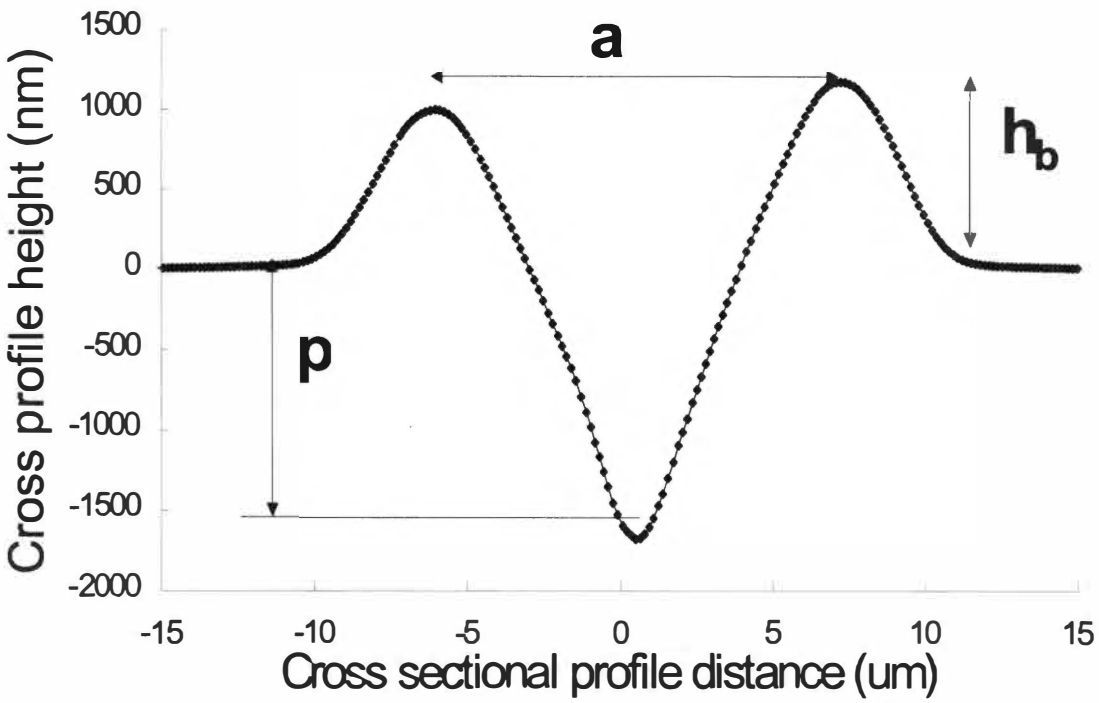


Figure 11: Cross sectional profile PMMA after a scratch was made at 100°C and 30mN load.

Scratch residual depth **p**: The height between the nominal surface and the bottom of the groove.

Scratch pile-up height h_b: The height of the peak of the pile-up above the nominal surface.

The scratch hardness H_S, has been defined by analogy to the indentation hardness by Briscoe [20] as:

$$H_S = \frac{F_N}{A_n} \qquad \textbf{Equation 1}$$

Where F_N is the force normal to the surface and A_N is the projected area (to be discussed shortly). The scratch hardness does not take the friction into account. The above parameters can be measured and calculated by performing a cross sectional profile of the scratch (Figure 11).

Gauthier and Schirrer et al [23, 24, 25] studied the transition between elastic and plastic deformation during scratch testing. Xie and Hawthorne [26] have used the transition between elastic and plastic behavior to obtain the yield stress of the material. The simultaneous occurrence of these two types of deformation influences the projected contact area between the scratch tip and

the surface. The cross sectional area of the scratch tip in contact with the material at the nominal surface, is defined as the projected contact area $\mathbf{A_n}$ (Figure 12).

Consider a scratch tip that has a spherical shape. If the contact is fully elastic, the contact area will be a full circle that recovers entirely behind the scratch tip. For a fully plastic contact, the material is permanently deformed and the area of contact will be half a circle (Figure 12) [24, 25] with area $\mathbf{A_N}$ given by:

$$A_N = \frac{1}{2}\pi\frac{a^2}{4} \qquad \textbf{Equation 2}$$

If the contact is developed by both elastic and plastic deformation, the contact area is modified by elastic recovery behind the scratch tip (Figure 13). This contact area is a very important parameter in scratch testing. To a first approximation it is given by area of a half circle. However, Gauthier et al [25] have proposed to correct this approximation by adding, the area due to the elastic recovery. This is made possible by the in-situ observation of the contact area during scratching [23, 24, 25] and direct calculation of the contact area from observations.

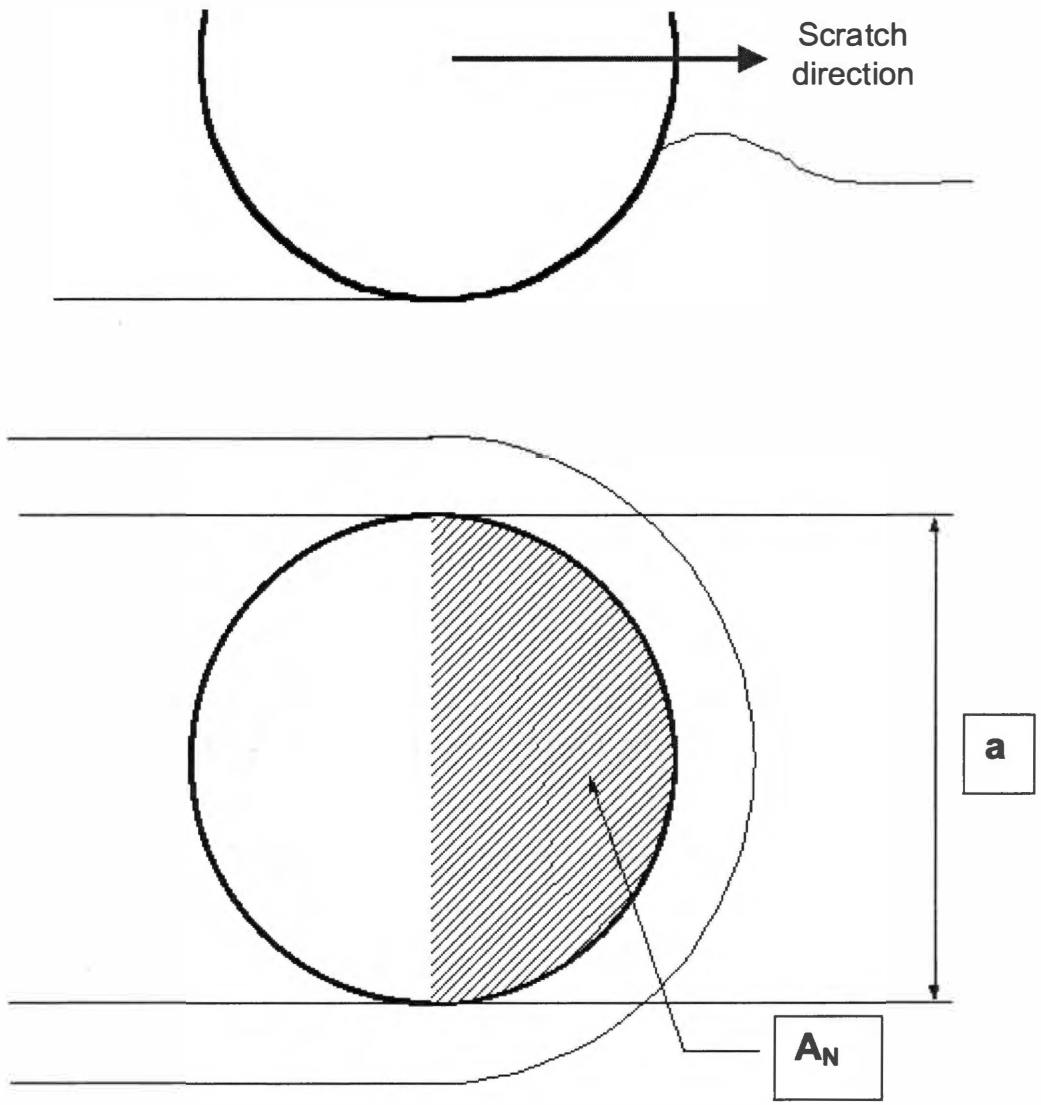


Figure 12: Contact area definition for a spherical scratch tip in the case of a fully developed plastic contact

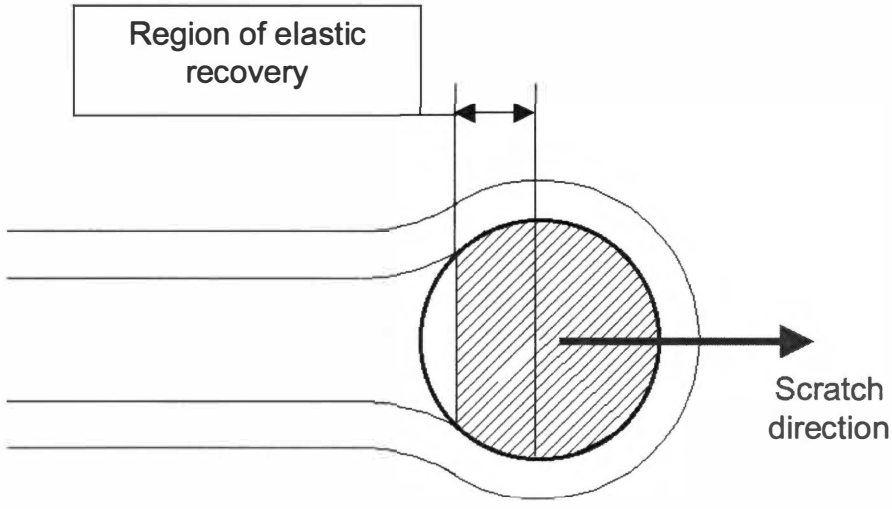


Figure 13: Contact area for the case of elastic-plastic contact

2.2.2 Fracture

In addition to elastic and plastic deterioration, scratching can also produce fracture. Fracture occurs when the material cannot support the stresses generated by the scratch tip. This phenomenon is very reproducible in scratch testing. The normal load, applied to the scratch tip at which the fracture occurs is called the critical load. This critical load is often used as a measure of the fracture resistance during scratching [17, 19, 27, 22].

The appearance of the fracture can be quite varied. From left to right on Figure 14, the fracture can be chevron-like, can cause chipping and removal of material, or can look like the material is flowing. When scratching a film on a substrate, one can also see, as in Figure 15, the delamination and rupture of the bond between the film and the substrate.

The scratch test has been used to study the fracture of thin films and bulk materials. Most of the testing methods lead to a ranking of the materials. The automotive paint industry uses the scratch test to estimate the influence of processing and aging parameters on the durability of the paints. Numerous

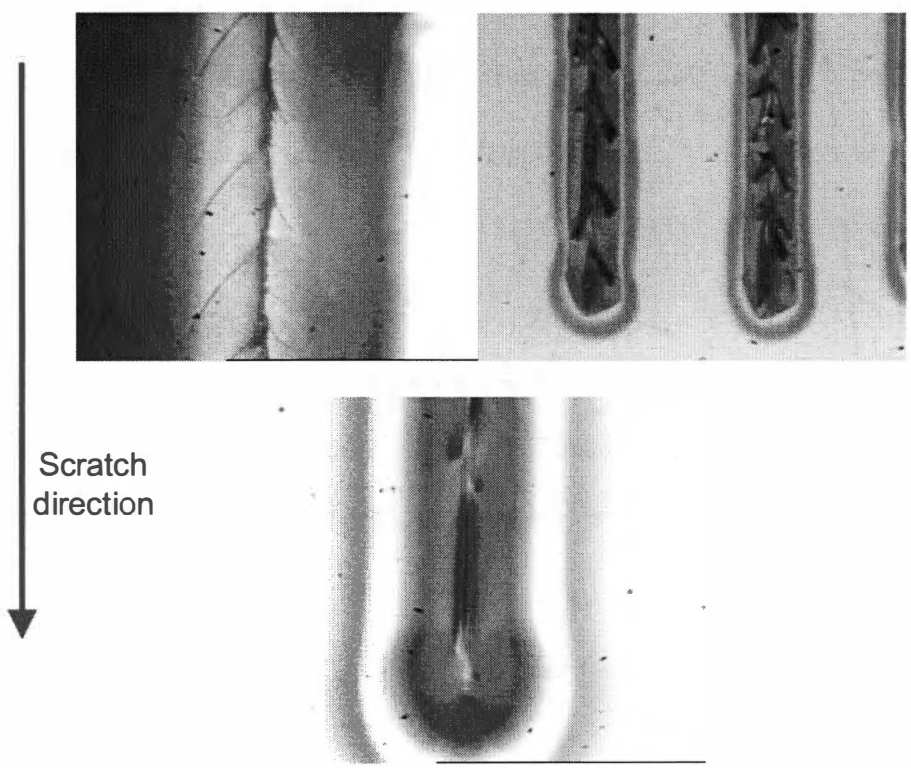


Figure 14: Different types of fracture during scratch testing of polymers.

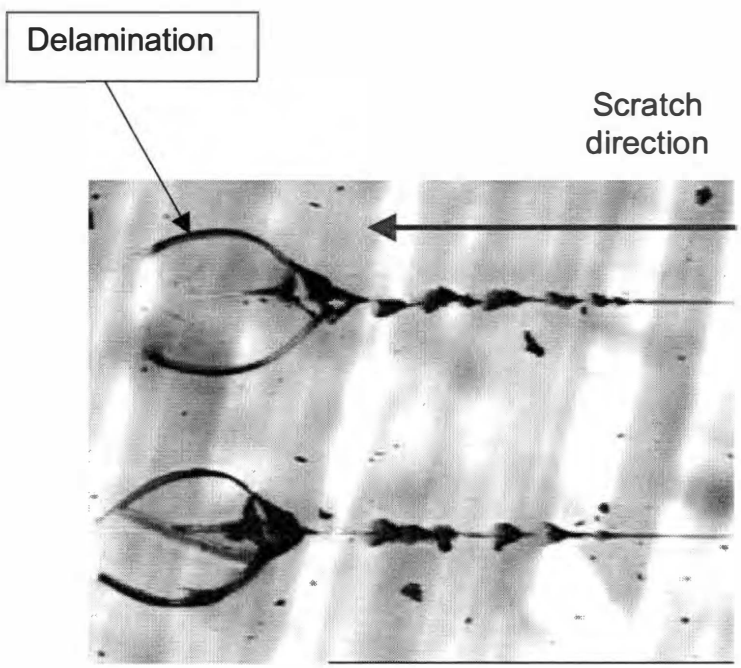


Figure 15: Delamination of a polymer film on a glass substrate

studies have been published on the scratch resistance of clear coats and automotive paints [28, 6, 7, 11, 8, 4, 9, 29, 13, 15].

N.X Randall et al. and Jardet et al. have studied the effect of material deterioration parameters on the fracture process [30, 17]. Briscoe has studied the influence of strain on the fracture on polymers during scratching [20], Mathia and Lamy have performed similar studies on ceramics [19]. Fracture is primarily a result of the severity of the contact, and is primarily related to the attack angle (2.1.2) and the scratch tip geometry (1.1.2).

CHAPTER 3: INSTRUMENTS / EXPERIMENTS

3.1 Instrumentation

3.1.1 Overview of the Nano Indenter XP®

The apparatus used in this work was the Nano Indenter XP® (Figure 16) manufactured by MTS Nano Instruments. It was originally developed for depth sensing indentation, but its configuration allows scratch test experiments to be conducted at a small scale. It was used in this work for both depth sensing indentation and scratch experiments.

The Nano Indenter® XP head is load-controlled. The load is applied via a magnet/coil system in a direction normal to the sample surface. This electromagnetic device allows for great precision and rapid control of the load. The indenter/scratch tip is located at the bottom of a column held in position by two leaf springs. This gives the system a very low vertical stiffness, but keeps a high lateral stiffness to restrain lateral motion of the column. The maximum vertical displacement of the column is 1.5 mm and the maximum applied load is 500 mN for the standard system. The sample is fixed on a sample tray that can

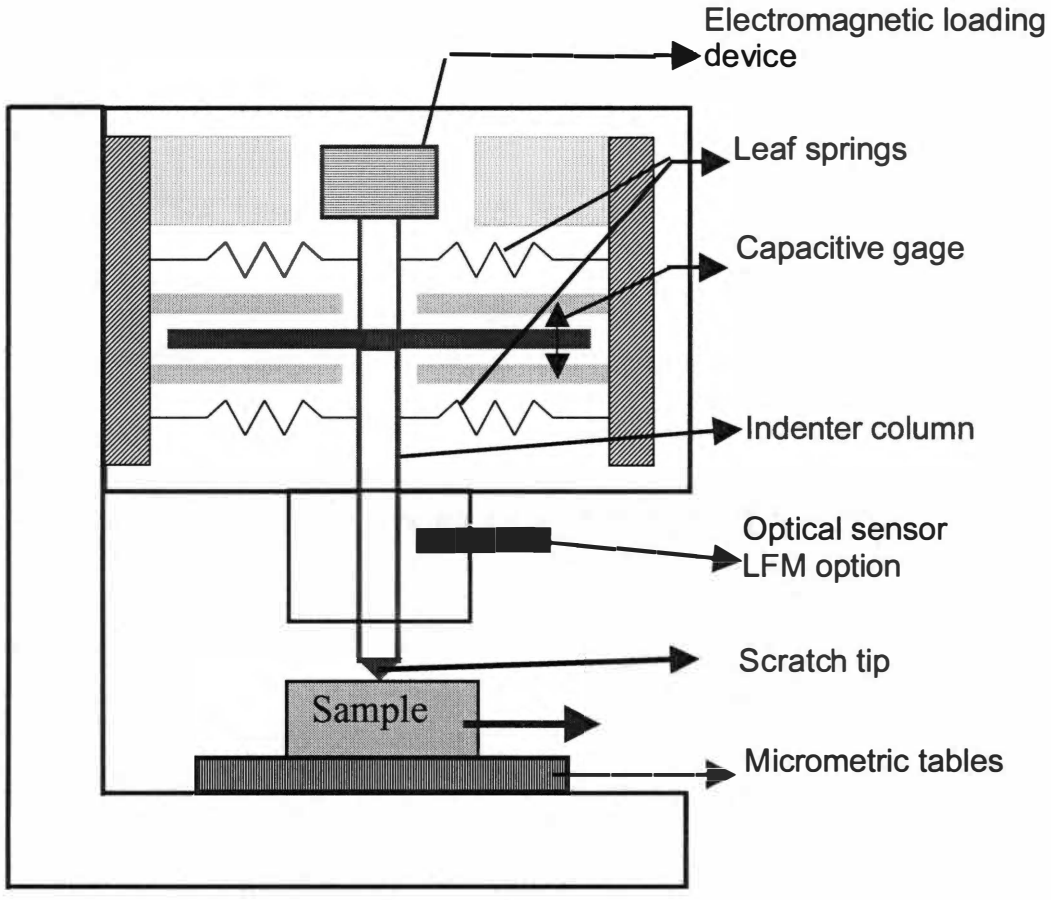


Figure 16: Schematic diagram of a Nano Indenter® XP with scratch testing capability

be moved with micrometric tables that give high positioning precision in the two horizontal directions. System specifications are given in Table 1 and Table 2.

3.1.2 Dynamic property measurement

The dynamic properties of the materials can be measured by indentation using the Continuous Stiffness Measurement (CSM) option. The principle of the CSM is to add a small amplitude oscillation to the continuous load signal. Analysis of this signal in relation to the signal coming from the displacement of the tip gives the dynamic stiffness, S and the contact damping, D, as a function of the penetration into the surface [43]. These dynamic measurements allow the calculation of the loss modulus **E"**, storage modulus **E',** and **tangent** δ, using the following equations [44]:

$$E' = \frac{\sqrt{\pi}}{2}\frac{S}{\sqrt{A}} \qquad \textbf{Equation 3}$$

$$E'' = \frac{\sqrt{\pi}}{2}\frac{D\omega}{\sqrt{A}} \qquad \textbf{Equation 4}$$

Table 1: Indentation Specifications for the Nano Indenter XP

Normal maximum load:	500 mN
Normal force resolution:	50nN
Maximum indentation depth:	1mm
Displacement resolution:	< 0.02 nm

Table 2: Scratch test Specifications for the Nano Indenter XP

Scratch speed:	0.1μm/s → 2.5mm/s
Scratch length:	10μm → 100mm
Maximum lateral force:	250mN (All direction)
Lateral force resolution:	2μN
Lateral force Noise level:	< 50 μN (without contact)
Scratch orientation:	0° → 360°

$$\tan\delta = \frac{E''}{E'}$$ **Equation 5**

$$H = \frac{P}{A}$$ **Equation 6**

Where **S** is the dynamic stiffness of contact,

D is the contact damping,

ω is the angular frequency of the oscillation,

A is the area of contact,

H is the indentation hardness

P is the load

The strain rate applied during indentation has been defined by Barry Lucas [36].

When the hardness is constant during the experiment:

$$\dot{\varepsilon}_i = \frac{\dot{h}}{h} = \frac{1\dot{P}}{2P}$$ **Equation 7**

Where P is the load and h the indenter penetration. Indentation tests in this work were performed at a constant value of $\frac{\dot{P}}{P}$=0.1. $nm.nm^{-1}.sec^{-1}$.

3.1.3 Temperature capability

The entire Nano Indenter® XP can be installed in a temperature chamber manufactured by THERMOTRON to perform the tests at temperature. In this chamber, the temperature is controlled with a precision of 0.1°C over the range of operation (-50°C to 100°C). Before and after each test (indentation or scratch), the temperature of the chamber is recorded. The temperature is adjusted before starting a new test and the temperature regulation system is turned off to avoid any noise or vibration during the experiment.

3.1.4 Scratch test experiments

3.1.4.1 Scratch testing procedure

Scratch tests were performed by moving the micrometric tables that carry the sample while the indentation head controls the load applied to the sample via the indenter. During a scratch test, the normal force applied to the sample can

be held constant, increased, or decreased. A typical scratch test in this work consisted of four parts:

- ✓ First, a profiling of the surface was performed under a very small load (20 μN), in order to record the original morphology of the surface before the scratch was made.
- ✓ Then, as the scratch tip was moved along the same path at a constant velocity, the normal load was increased linearly from 20 μN to the maximum load to create the scratch.
- ✓ A post scratch profile was performed along the same path, under a very small load (20 μN), to measure the residual deformation in the groove.
- ✓ Finally, a profile across the scratch groove was made to give the shape of the groove and evaluate the extent of plastic deformation.

A summary of the scratch procedure is given in Figure 17.

3.1.4.2 Relation between scratch and indentation measurements

The equivalence of the contact pressure in a scratch test and hardness in indentation test has been shown in room temperature experiments by Jardret,

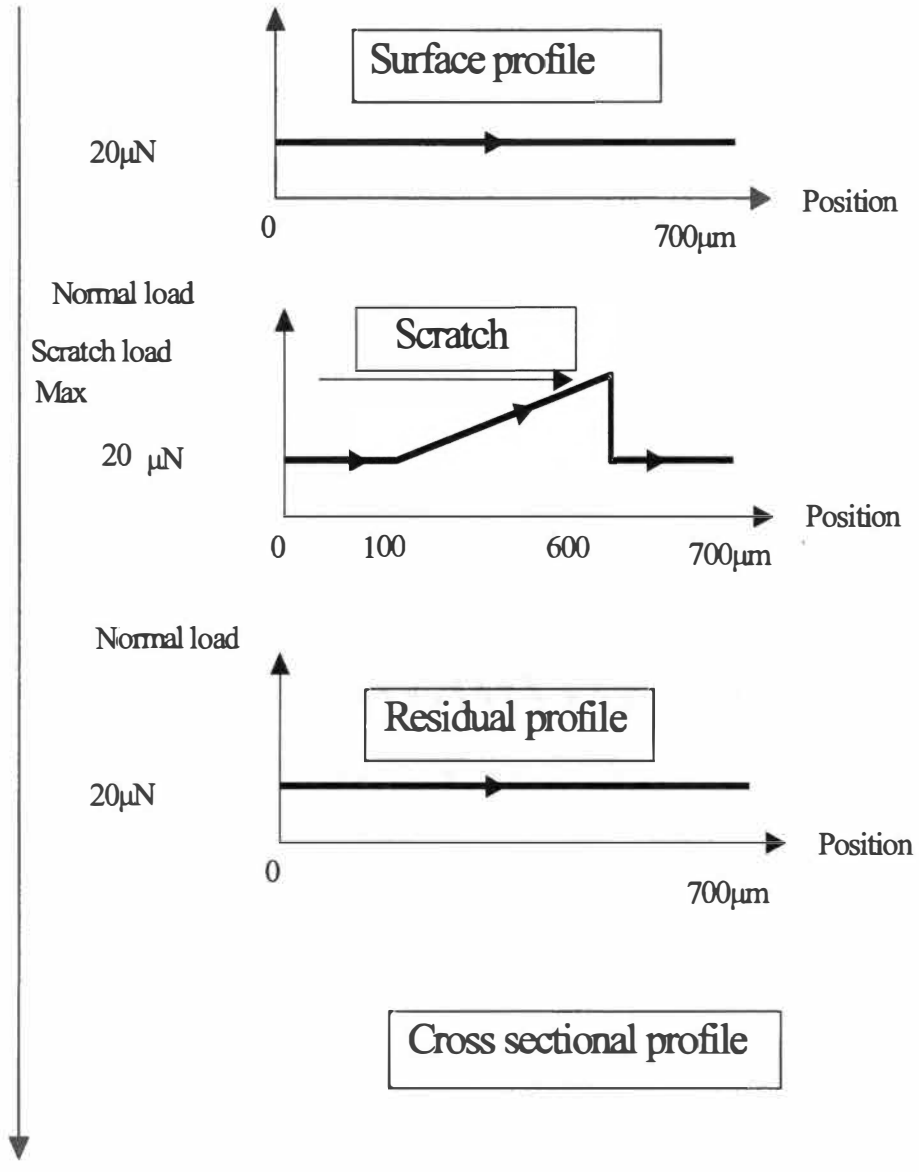


Figure 17: The four main parts of the scratch testing procedure

Zahouani, Loubet, and Mathia [31]. The study of Jardret and Oliver [18] showed an increase of the hardness when the strain rate is increased for room temperature scratching.

Briscoe [39] and Gauthier and Schirrer [23, 24, 25] established that the strain rate in a scratch test can be defined as:

$$\dot{\varepsilon}_S = \frac{Vtip}{a} \qquad \textbf{Equation 8}$$

Where $\mathbf{V_{tip}}$ is the scratch velocity and **a** is the scratch width.

In an indentation test, the hardness is defined as

$$H = P_m / A \qquad \textbf{Equation 9}$$

where **P** is the maximum load and **A** the area of contact [32, 33].

For the scratch test the contact pressure, or scratch hardness, is estimated by:

$$H_s = q\frac{4F_n}{\pi a^2} \quad \textbf{[34, 20, 31]} \qquad \textbf{Equation 10}$$

where F_n is the normal load, **a** is the residual scratch width, and **q** is a material coefficient equal to one in this study of PMMA.

3.1.4.3 Lateral force measurement

The Lateral Force Measurement (LFM) option of the Nano Indenter XP® allows the measurement of the forces in the X-Y horizontal plane. During a scratch test these forces correspond to the tangential friction force and to the lateral scratch force as defined in Figure 18. These forces are obtained by measuring optically the lateral displacement of the indenter column in two orthogonal directions (X and Y). Knowing the lateral stiffness of the column assembly and the lateral displacement, one can calculate the lateral force applied to the column.

3.2 Indenter geometry characterization

Due to the small size of the indenter/scratch tip, it is difficult to manufacture certain geometrical shapes like a cone without rounding at the tip. That is why conical tips are usually defined by the included angle of the cone **α**, and the estimated radius of the tip rounding **R** (Figure 19).

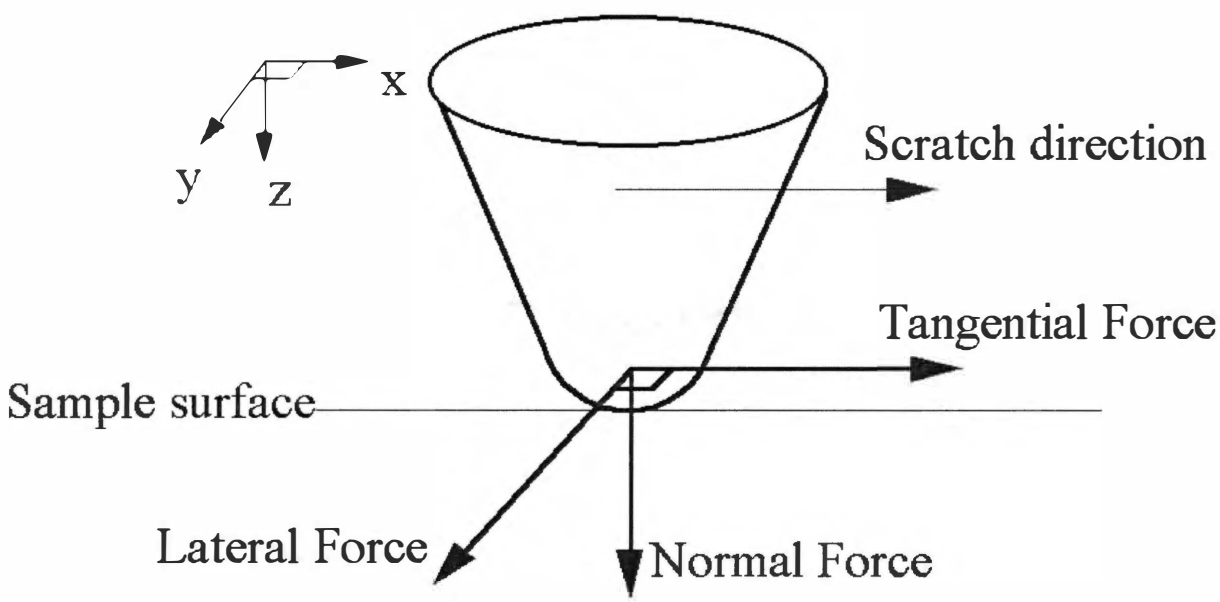


Figure 18: Forces during scratch testing

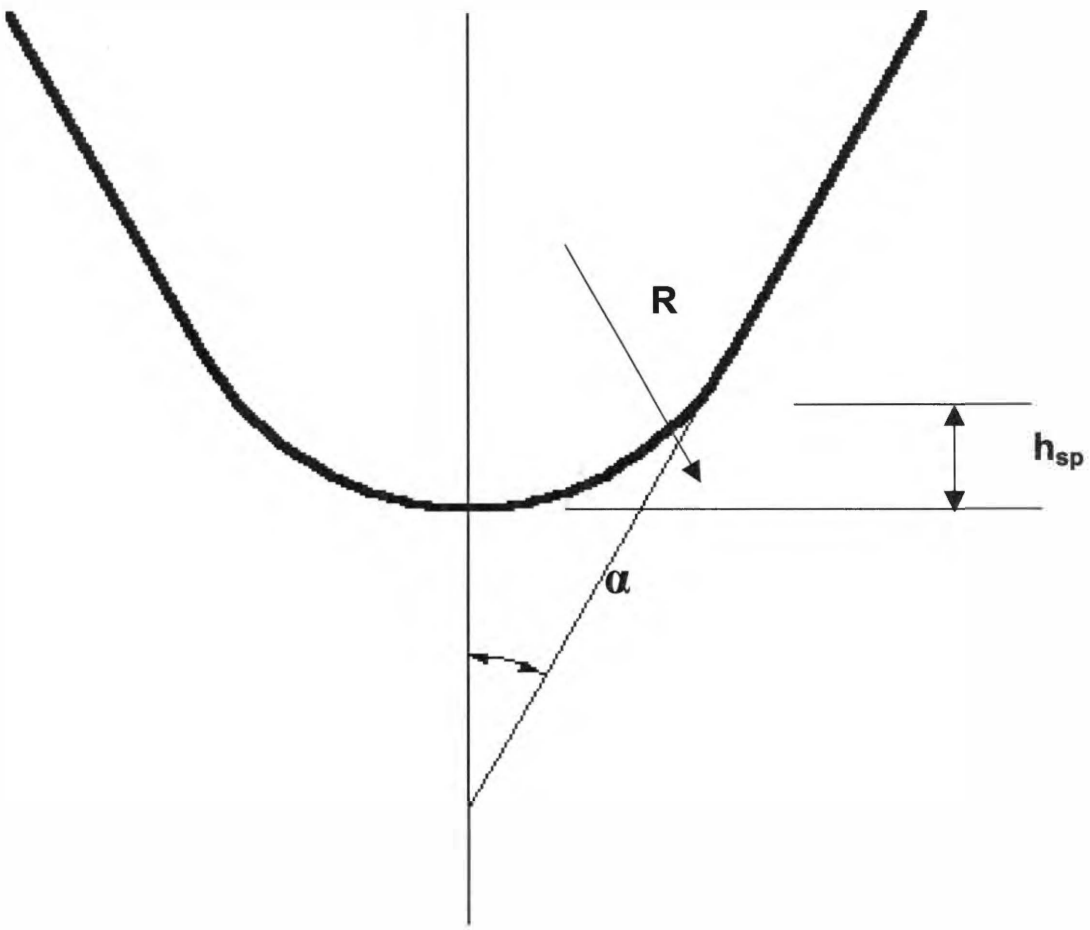


Figure 19: Characterization of the conical geometry of the indenter/scratch tip by a half included angle, α, and a tip radius, R.

In order to characterize precisely the shape of the indenter, indentation tests were conducted on a material for which the elastic modulus is well known. Fused silica is commonly used for this purpose. The spherical part of the tip can be characterized by looking at the evolution of the equivalent indenter width, or contact radius, compared to the indenter height (Figure 20). The measurement of the elastic contact stiffness as a function of contact depth describes the indenter geometry.

Pharr, Oliver, Brotzen [35] have shown that the modulus **E** of a material as a function of the stiffness of the contact **S** and the area of contact **A** in indentation is given by:

$$E = \frac{\sqrt{\pi}}{2}\frac{S}{\sqrt{A}} \qquad \textbf{Equation 11}$$

From this relation, and assuming that the contact area is a circle in the case of a conical indenter, the radius of contact r_c can be expressed:

$$r_c = \frac{S}{2E} \qquad \textbf{Equation 12}$$

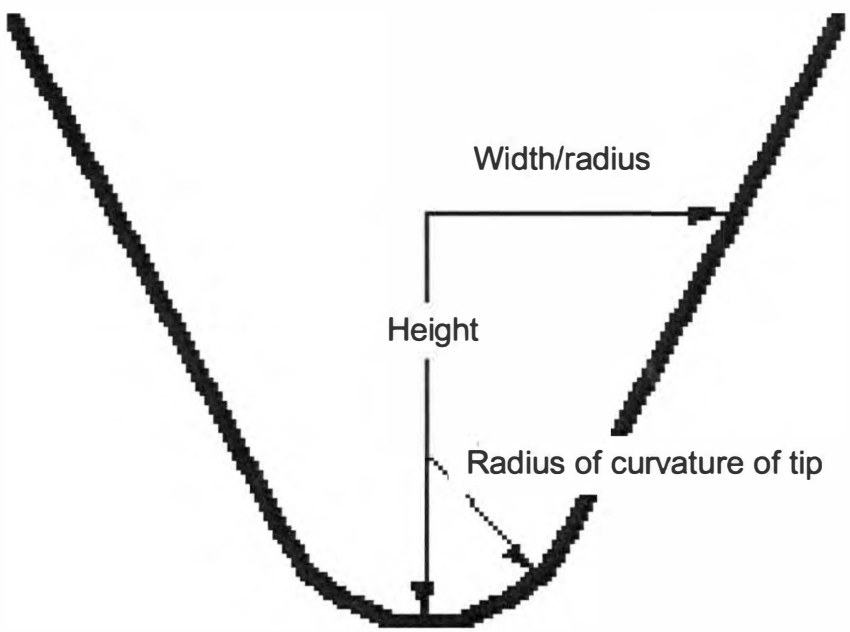


Figure 20: Relationship between the height and width of the scratch tip

One can then plot the radius as a function of depth to obtain the shape of the tip.

3.3 Critical load and Fracture analysis

As defined previously (section 2.2.2) the critical load is that at which the material starts to fracture. During an experiment, the load is increased linearly and its value is recorded as a function of the distance along the scratch path. The value of the critical load is determined by analyzing data after the test. When particles are chipped out of the surface and/or cracks appear in and/or outside the scratch, there is a sudden movement of the scratch tip that can be seen as irregularities in the scratch penetration, and tangential force curves and the residual scratch morphology. The critical load value is taken at the point showing the first indications of irregularities. The critical load value can also been confirmed by an optical observation of the scratch track and a length measurement along the scratch track. This is illustrated for a scratch in PMMA in Figure 21. The plot shows the vertical penetration of the scratch tip during the scratch segment and the post profile segment. Fracture indications are present in both. One has to keep in mind that the critical load is very dependent upon the indenter/scratch tip shape. This is due to the fact that the geometry and the

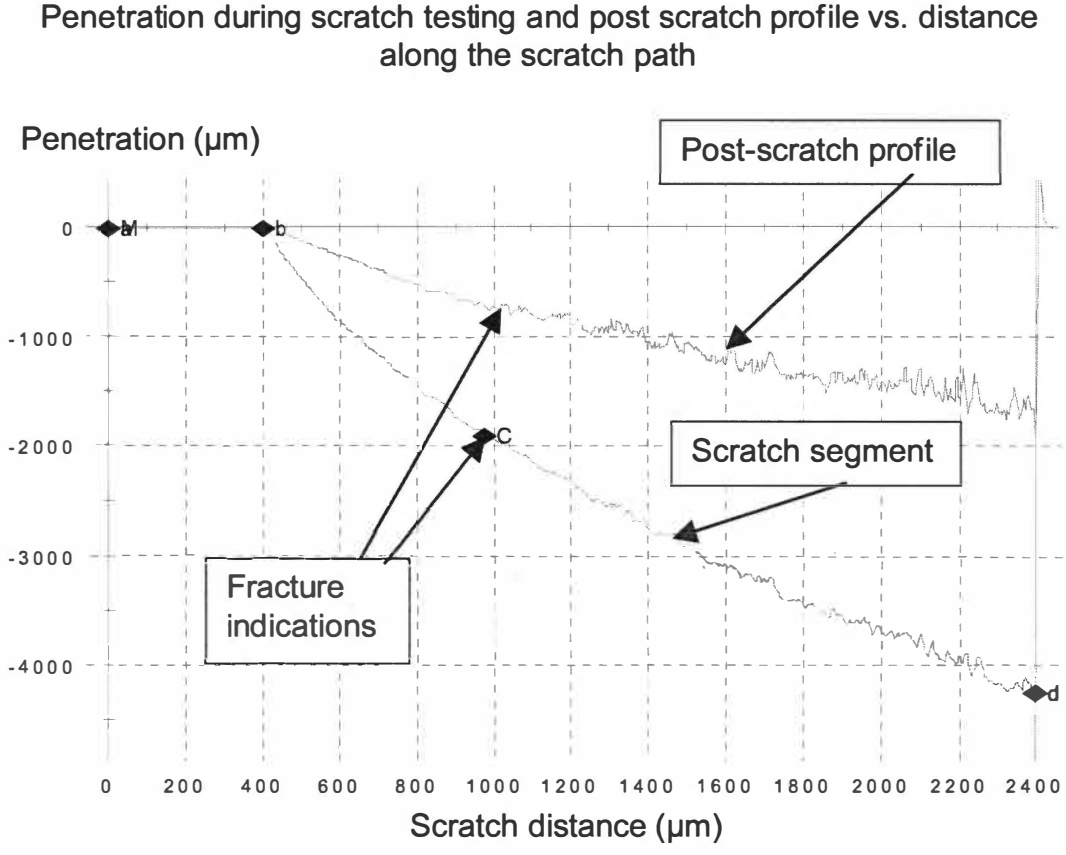


Figure 21: Indications of fracture on the post scratch profile and the scratch segment data

attack angle are parameters that play an important role in determining the stresses applied to the material.

The shape of the fracture is also a very important parameter. The fracture shape provides information about how the fracture happened. Optical observations of different types of fracture are shown in Figure 22 to Figure 25. In Figure 22 the fracture during scratching caused chipping and removal of material. Small cracks appear in the fracture shown in Figure 23. A cube corner tip pulls out a lot of material (Figure 24). Scratching a thin film can cause delamination as illustrated in Figure 25.

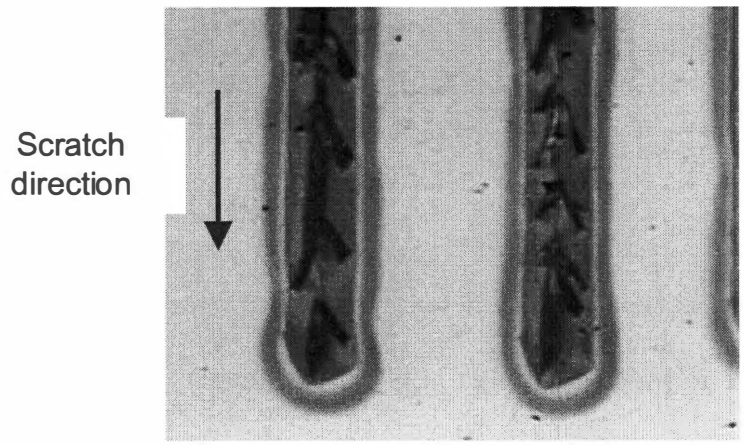


Figure 22:Fracture obtained with a 60° cone on a compound polymer coating (unknown composition).

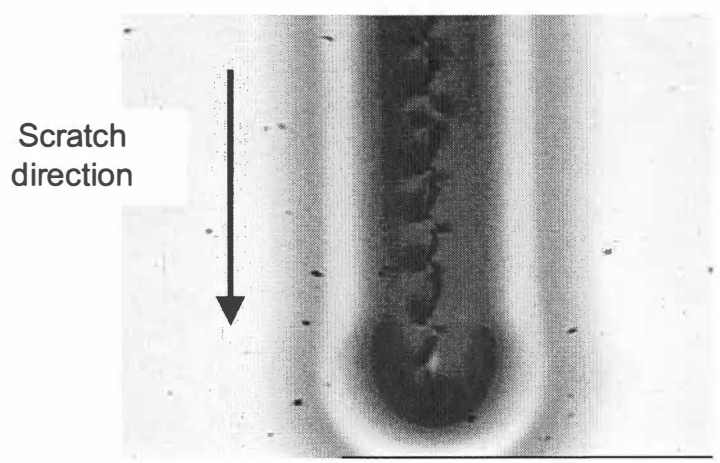


Figure 23: Fracture of PMMA at 80°C, obtained with a 90° cone and a 100mN load.

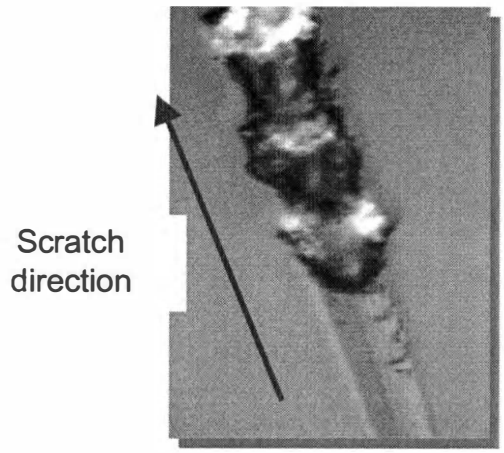


Figure 24: Fracture obtained with a cube corner on automotive paint.

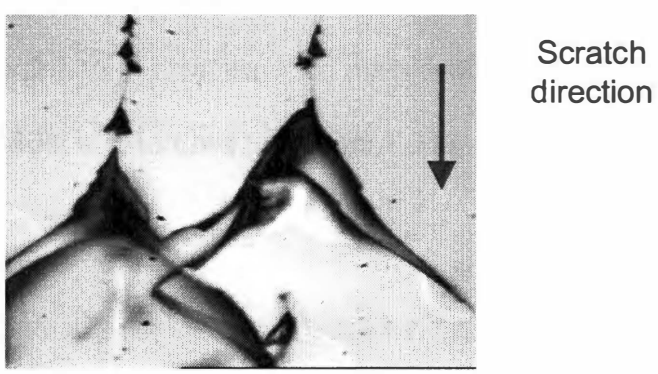


Figure 25: Fracture and delamination of a polymer compound (unknown composition) on a glass substrate due to scratching with a 60° cone.

CHAPTER 4: EXPERIMENTAL RESULTS AND DISCUSSION

Polymers exhibit a transition in mechanical behavior around their glass transition temperature. In order to observe a change in behavior in the range of temperatures available for indentation and scratch tests, the polymer material must have a transition in the range of temperature available to the Nano Indenter XP® in the THERMOTRON chamber (between 0°C and 100°C). PMMA (poly-methylmethacrylate), an amorphous thermoplastic, has a transition close to this range (around 110°C), and is glassy at room temperature. Furthermore, numerous studies on this material have provided a great deal of information on its visco-elastic properties, the loss and storage modulii and the stress strain behavior as a function of temperature [38]

4.1 Indentation results as a function of temperature

Indentation tests provided basic information on the elastic modulii and hardness as a function of temperature. The loss and storage modulii, the hardness, and tan δ are obtained using CSM data and the equations presented in section 3.1.2. A Berkovich indenter was used for the indentation tests, which were performed between 5ºC and 90ºC.

Figure 26 shows that there is a decrease in the storage modulus and hardness as the temperature is increased. Over the same range of temperature, the loss modulus increases slightly, which leads to an increase in Tan δ (Figure 27). The combined observations suggest that the glass transition would be at higher temperature. For PMMA the glass transition is at 110°C at 1 Hz. One can notice that the storage modulus obtained with indentation test at room temperature (5 Gpa) is higher that the values given by DMA testing at 1 Hz, in the literature (3.5 Gpa).

4.2 Scratch results as a function of temperature

Since the scratch resistance is mainly determined by plastic deformation and fracture behavior, differences between ductile and brittle behavior in the scratch test can be characterized by several important parameters. Ductile deformation during scratching is evaluated through the contact pressure, the residual groove depth, and the height of the pile-up. The applied load at which the fracture occurs, the critical load is the basic measure of the fracture resistance.

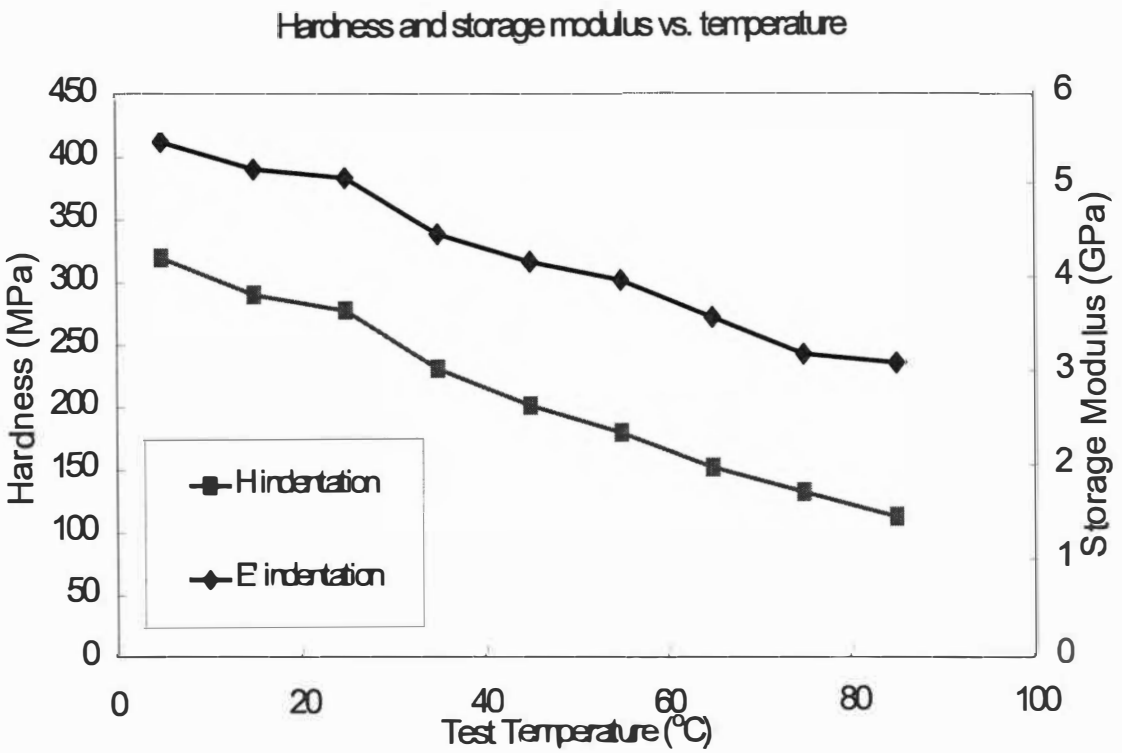


Figure 26: Effect of temperature on hardness and storage modulus for PMMA

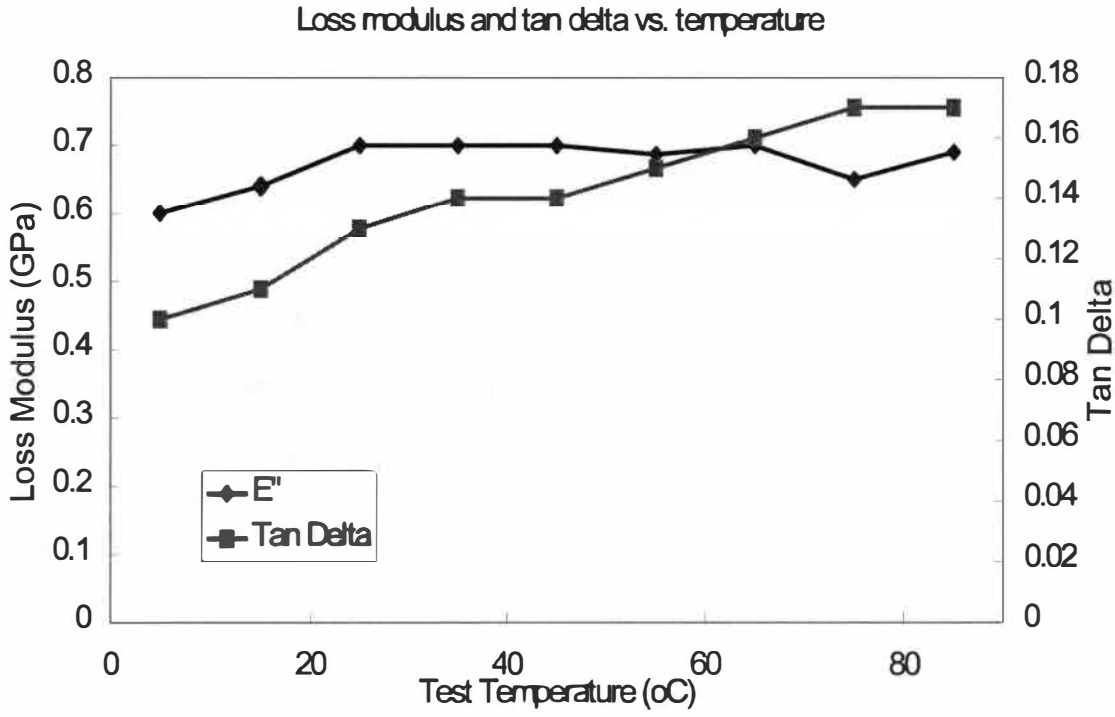


Figure 27: Effect of temperature on loss modulus and tan δ for PMMA

4.2.1 Relation with mechanical properties

Figure 28 compares the temperature dependence of the indentation and scratch hardnesses. The indentation tests were conducted with a Berkovich indenter and the scratch tests with a 90° cone with a 2 μm radius tip. The hardnesses were computed using the contact areas determined from **Equation 9** and **Equation 10**, which take the tip geometries into account.

The difference in values between the indentation hardness (**Equation 9**) and the scratch hardness (**Equation 10**) in Figure 28 is due to the difference in strain rate between the two different experiments. Jardret and Oliver [18] have shown, for different tip geometries, that at same strain rate the indentation and scratch hardnesses are the same. The two different values of strain rate, obtained with **Equation 8** and **Equation 7**, are shown in the Figure 28.

Plastic deformation during scratch testing is commonly measured by the pile-up height and the residual depth of the scratch. The plastic deformation produced during indentation testing and scratch testing depends on the relative magnitude of the elastic and plastic properties of the material. The pile-up height is related to both the modulus over hardness ratio and the indenter shape [37, 18] and varies with strain rate and temperature.

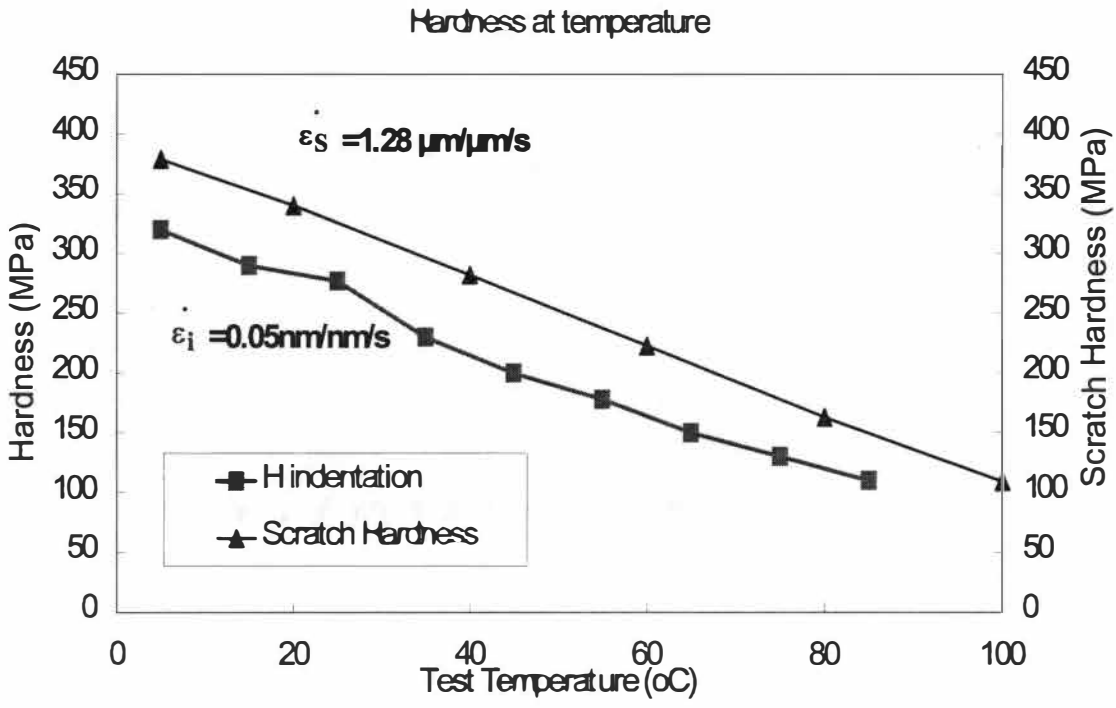


Figure 28: Dependence of indentation hardness and scratch hardness on temperature

The results in Figure 29 show the effect of temperature on the pile-up of scratched PMMA. Cross sectional profiles were performed at different positions along the scratch. This position is given by the value at the load achieved during the loading ramp along the scratch path shown in the legend on the right of the plot. The same positions are used at each temperature. On the same plot the ratio E/H from the indentation tests is plotted. Figure 29 shows a strong correlation between the pile up height and the ratio of the modulus to the hardness.

Jardret [31] showed a strong correlation between the pile-up height and the ratio E/H for a wide range of materials at room temperature. In this work, the same correlation is found at a variety of temperature.

The strain rate also has an effect on plastic deformation. **Equation 8** shows that the strain rate varies with the scratch speed. In order to obtain a variation in the strain rate, the scratch speed was varied at room temperature. The shape of the groove was measured at the same position along the scratch (50 mN) and at different scratch speeds (Figure 30). Higher strain rates lead to smaller widths and depths of the groove. Surprisingly, the height of the pile-up does not seem to be affected by the strain rate.

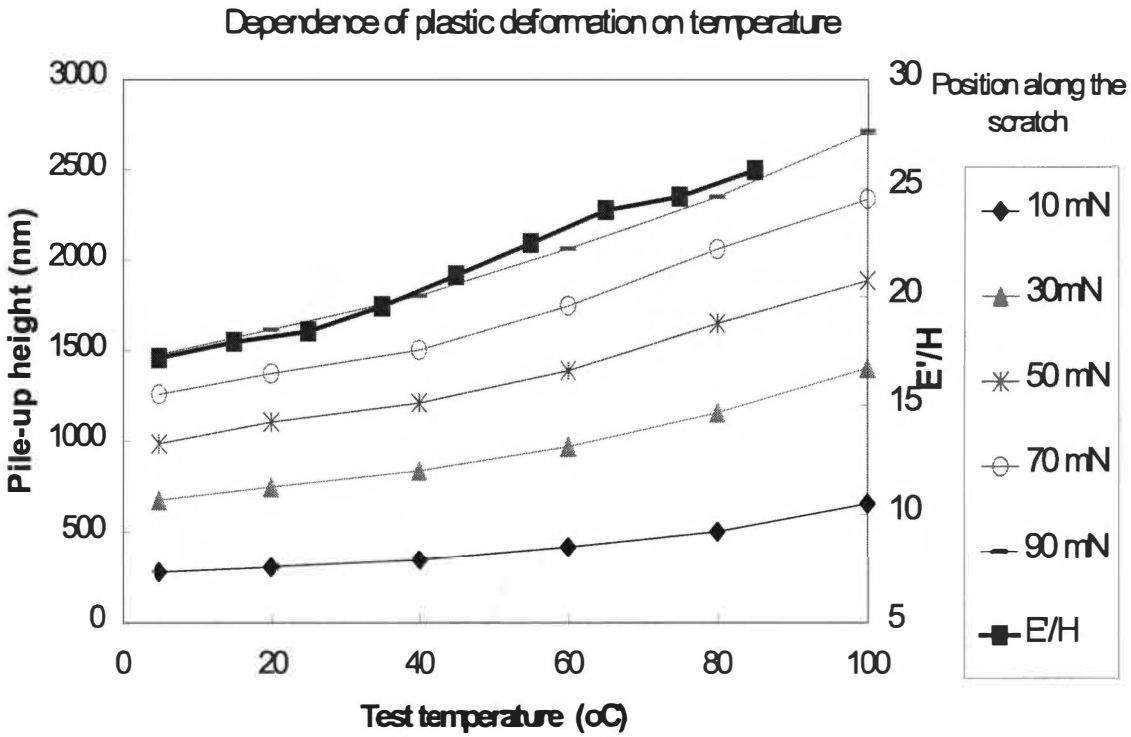


Figure 29: Dependence of pile-up height and the ratio E'/H, on temperature

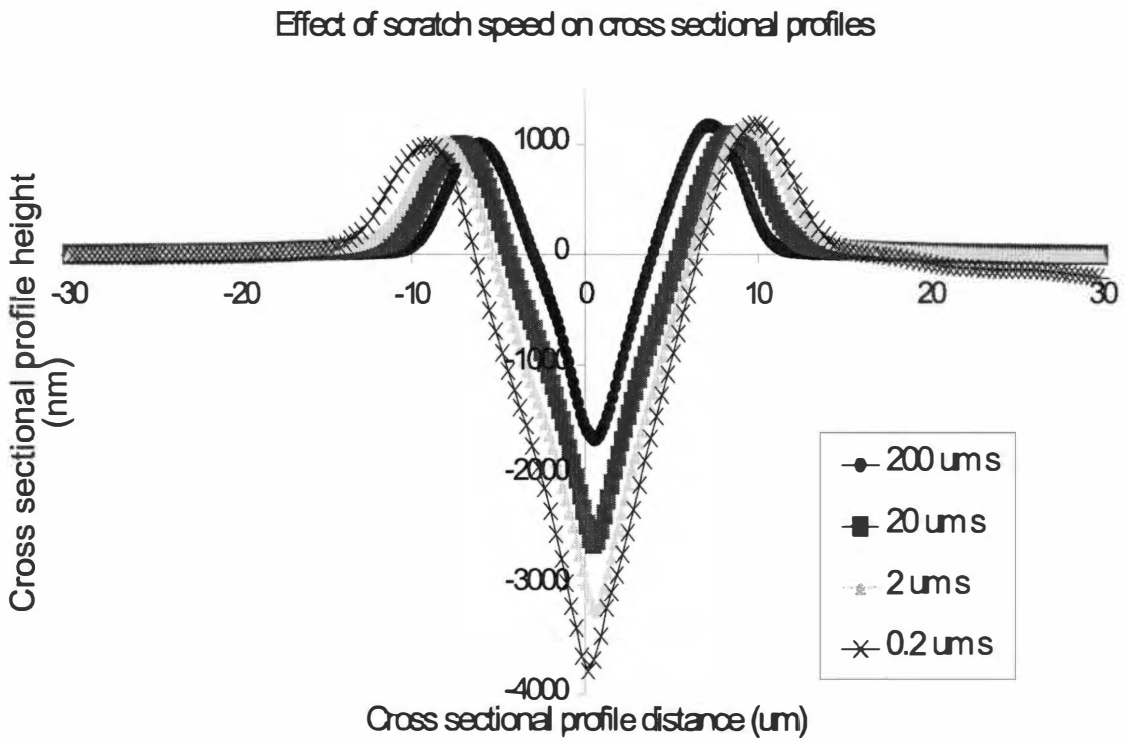


Figure 30: Cross sectional profiles at different scratch speed

4.2.2 Dependence of the critical load on temperature

The parameter most commonly used to describe the ductile to brittle transition in the scratch process is the critical load. The dependence of the critical load on temperature was studied in this work for the scratch tests performed on PMMA with a conical scratch tip with a 90° cone angle and 2 μm tip radius. Figure 31 shows the dependence of the critical load as a function of the temperature. The plot exhibits an inflection point around 50°C, which correlates with a change in fracture behavior. Fracture occurs at smaller loads for low temperatures and higher loads for high temperatures.

The optical micrographs of scratch tracks in Figure 32 show a change in the morphology of the fracture between high and low temperatures. Fracture is more extensive at low temperatures with a lot of missing material, whereas, at high temperatures, there is much less splintering on the sides of the scratch track and material seems to have plastically flowed. A closer look at the end of the scratch in Figure 33 shows that no fracture is present in front of the last position of the indenter. This indicates, as it has been observed in other work [16], that fracture occurs behind the contact.

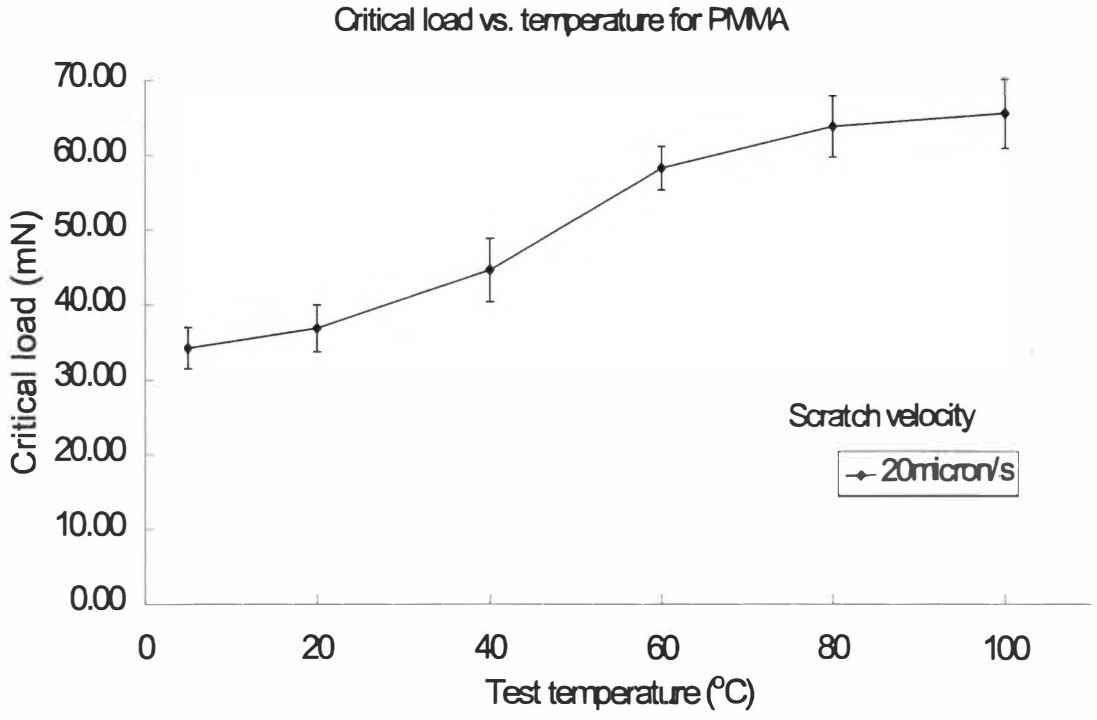


Figure 31: Dependence of critical load on temperature for scratch testing of PMMA

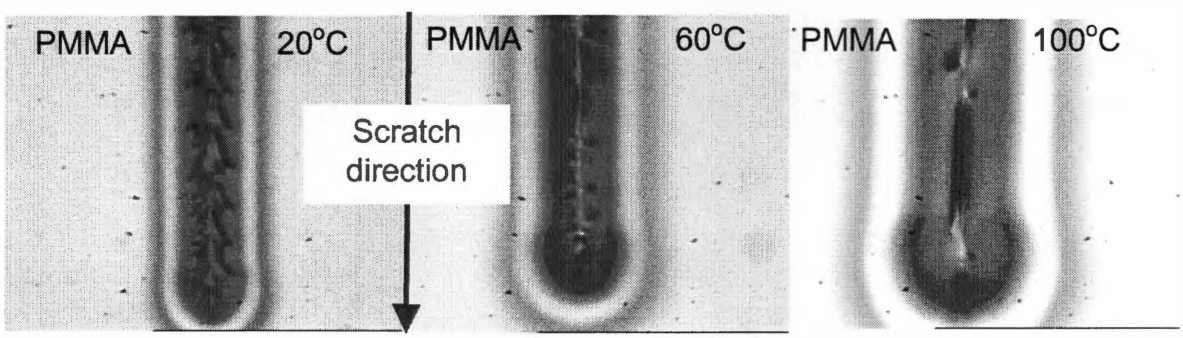


Figure 32: Observation of the fracture during scratch testing at different temperatures

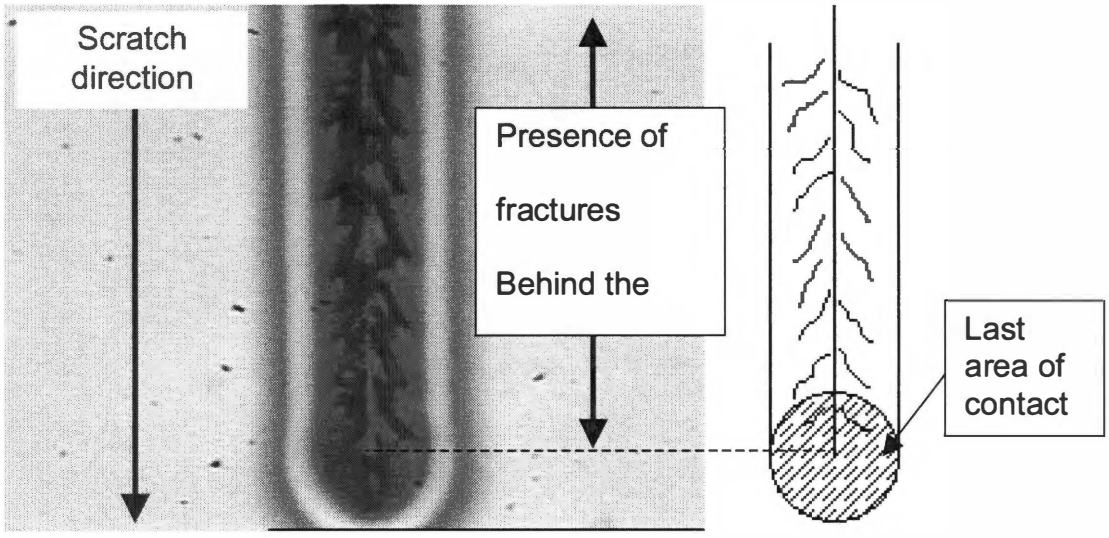


Figure 33: Optical micrograph of the end of the scratch track demonstrating that fracture occurs behind the contact.

4.2.3 Comparison of critical load to tensile behavior

In order to compare the fracture observations to known behavior for PMMA, the literature was searched for compression and tensile data [38].

The compression test curves in Figure 34 show that temperature has an effect on the steady state flow stress, with the flow stress being lower at higher temperatures. However, at all temperatures, the shape of the stress/strain curve is generally the same. The elastic modulus, which is the slope of the initial linear part of the curve, is changed by temperature. Different strain rates have also been applied during these compression experiments. An increase in the strain rate increases the magnitude of the flow stress.

As shown in Figure 35, temperature has a tremendous effect on the shape of the tensile curves. At low temperatures, PMMA behaves like a brittle material with very little plasticity and breaks at very low strains and high stresses. For the higher temperatures, PMMA behaves more like a rubber for which the fracture occurs at high strains and lower stresses. The first part of the high temperature curve represents the effect of straining on the Vander Waals bonds and the orientation of polymer molecules in the tensile direction. Subsequently, the stress is almost constant corresponding to the stress necessary just to

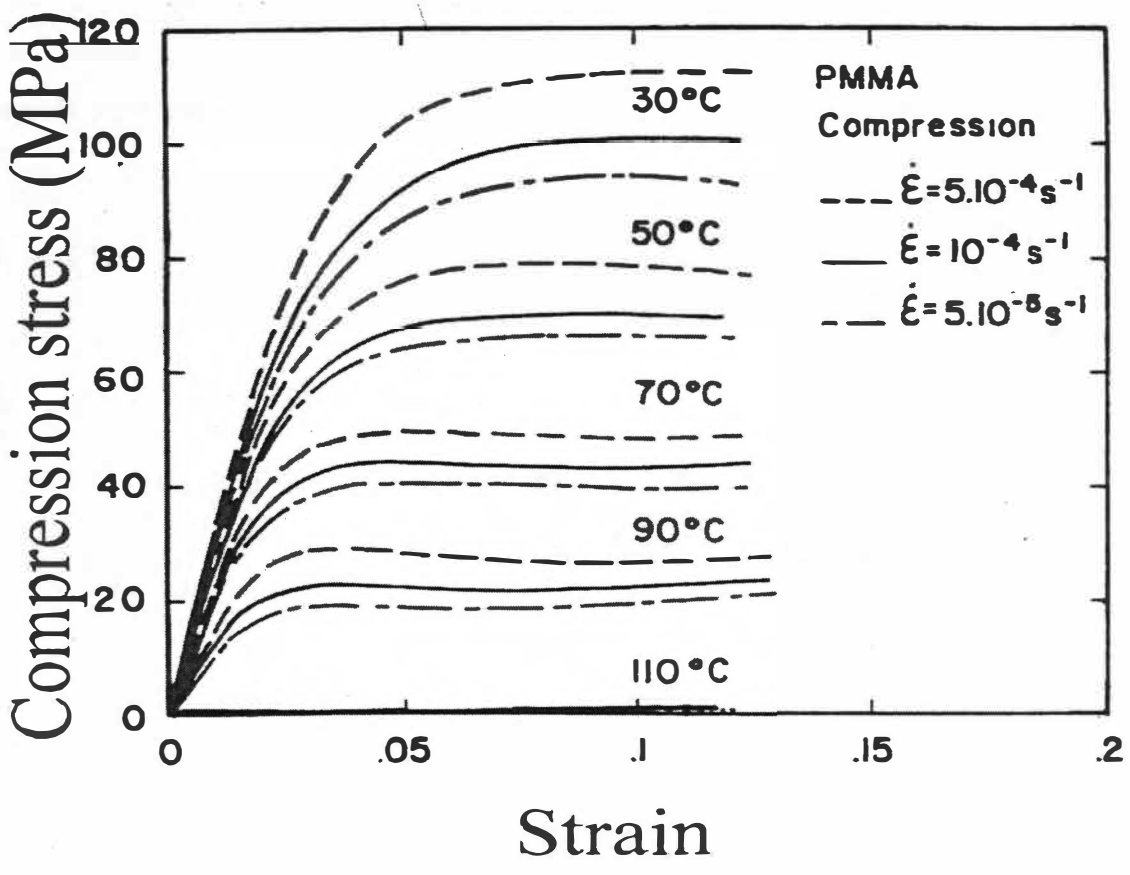


Figure 34: Stress/strain curves for PMMA in compression tests [38]

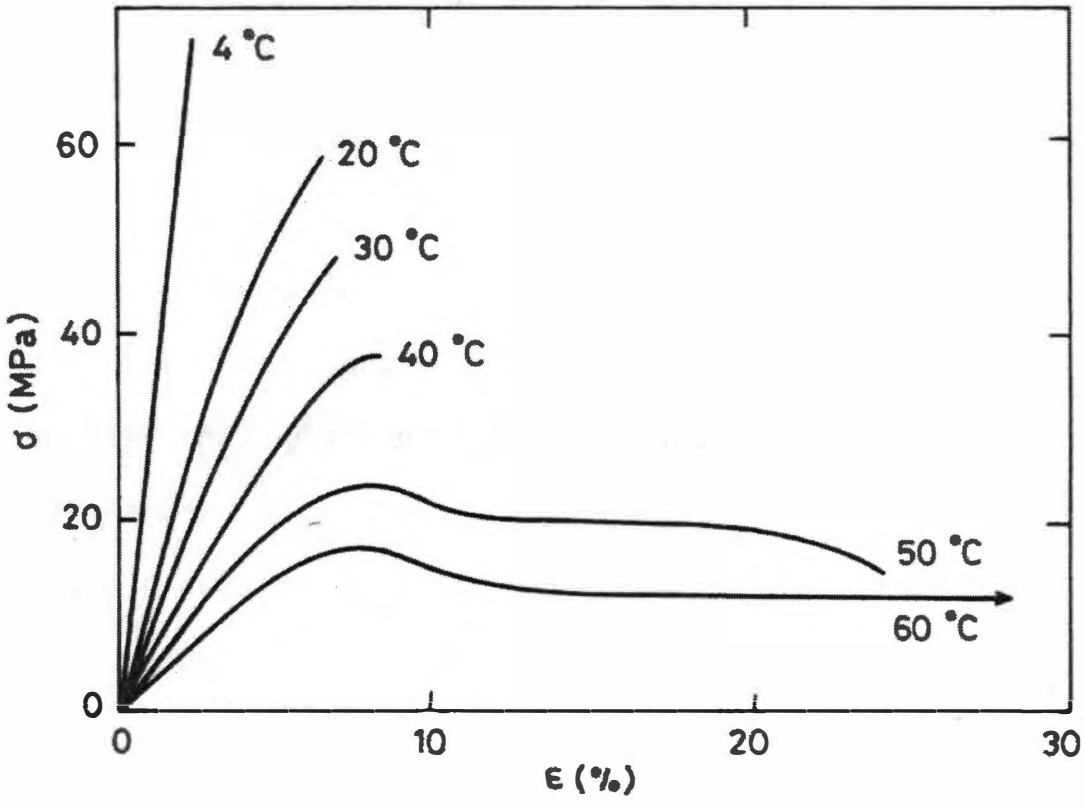


Figure 35: Stress/strain curves for PMMA in tensile tests [38]

uncoil the polymer chains. Ultimately, the stress would increase when covalent bonds of the polymer molecule are strained.

An important feature to note in Figure 35 is that the shape of the stress/strain curves changes around 50°C corresponding to the "brittle-ductile transition" [38]. This transition correlates well with the transition observed in the critical load during scratch testing (Figure 31). This suggests that the fracture mechanisms in scratch testing and tensile testing are similar.

There is also data in the literature for the temperature dependence of the yield stress σ_Y and fracture strength (stress required to cause brittle fracture) σ_B. Figure 36 illustrates schematically that brittle fracture and yield are two independent processes that are temperature dependent. Both the yield stress and fracture strength decrease with temperature, and there is a transition temperature at which $\sigma_Y = \sigma_B$. Below this transition temperature, the yield stress is higher than the fracture stress and fracture dominates. Above the transition temperature, the situation is reversed leading to yielding and ductile behavior. The temperature at the intersection of the two slopes is the brittle-ductile transition temperature, which suggests the existence of a transition between brittle and viscoplastic behavior. Collectively, the data in Figure 34, Figure 35 and Figure 36 relate the behavior of PMMA behavior during scratch testing to its tensile behavior. One has to keep in mind the strong

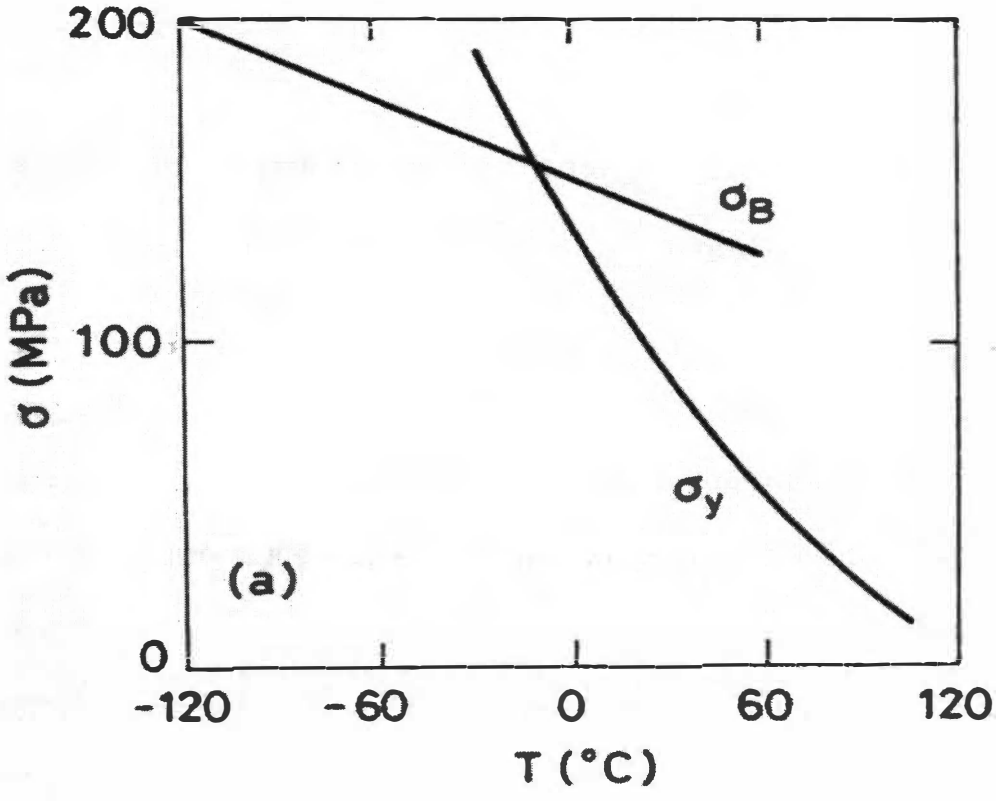


Figure 36: Temperature dependence of σ_Y (yield stress) and σ_B (stress required to cause brittle fracture) for PMMA [38]. Note that the strain rate has a strong influence on the position of the transition temperature (shown in Figure 39).

effect of the strain rate on the transition temperature as illustrated later in Figure 39. This leads to a hypothesis that may explain the origin of fracture in the scratch test.

4.2.4 Hypothesis for the origin of fracture during scratch testing

It has been suggested that fracture during scratch testing is due to tensile tearing [16]. Results in this study, point out a very strong correlation between the tensile behavior of the PMMA and the fracture behavior in scratch testing. This leads to an explanation for the fracture origin, which is schematically described in Figure 37. A compression zone is created ahead of the scratch that compresses material in front of the scratch tip, while tensile stresses develop behind the scratch tip. If these stresses reach the value of the fracture stress of the material, then fracture occurs.

This explanation is consistent with the fact that fracture is observed behind the contact area and that the critical load exhibits the same "brittle-ductile" transition as in tensile tests.

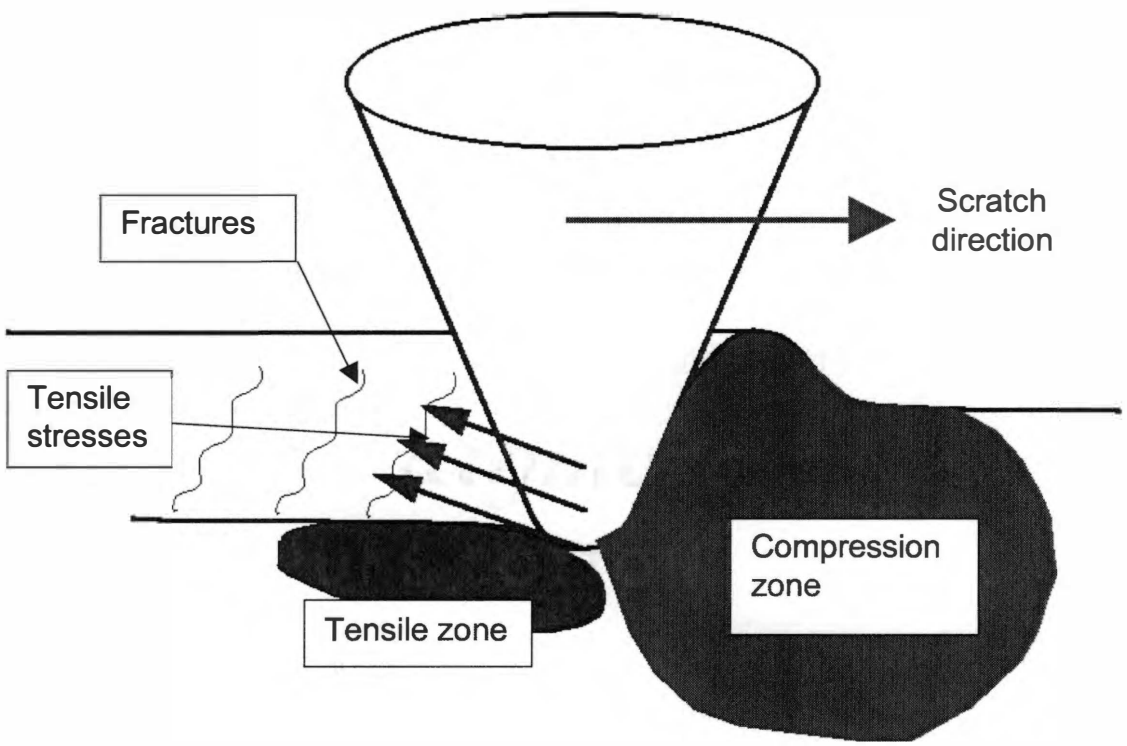


Figure 37: Explanation for the origin of fracture and stresses around the scratch tip

To summarize, the fracture behavior in scratch testing is linked to the tensile behavior of the material. The transition observed in the critical load as a function of the temperature occurs at a similar temperature as the one observed in the tensile behavior of the PMMA. Optical observation of the change in fracture behavior and comparison with the literature suggests that the fracture is generated by tensile stresses behind the indenter, but only when the temperatures are below the ductile-brittle transition.

4.3 Influence of Indenter shape on deformation behavior and strain rate

4.3.1 Geometrical considerations

In order to develop a better understanding of the effect of the scratch tip geometry on scratch deformation behavior, one has to first define several different geometric parameters. As shown in Figure 38 if **R** is the radius of the spherical part of the tip and **α** the half angle of the cone, the vertical height of the spherical part of the tip, $\mathbf{h_{sp}}$, can be calculated as:

$$\mathbf{h_{sp} = R(1 - \sin\alpha)} \qquad \textbf{Equation 13}$$

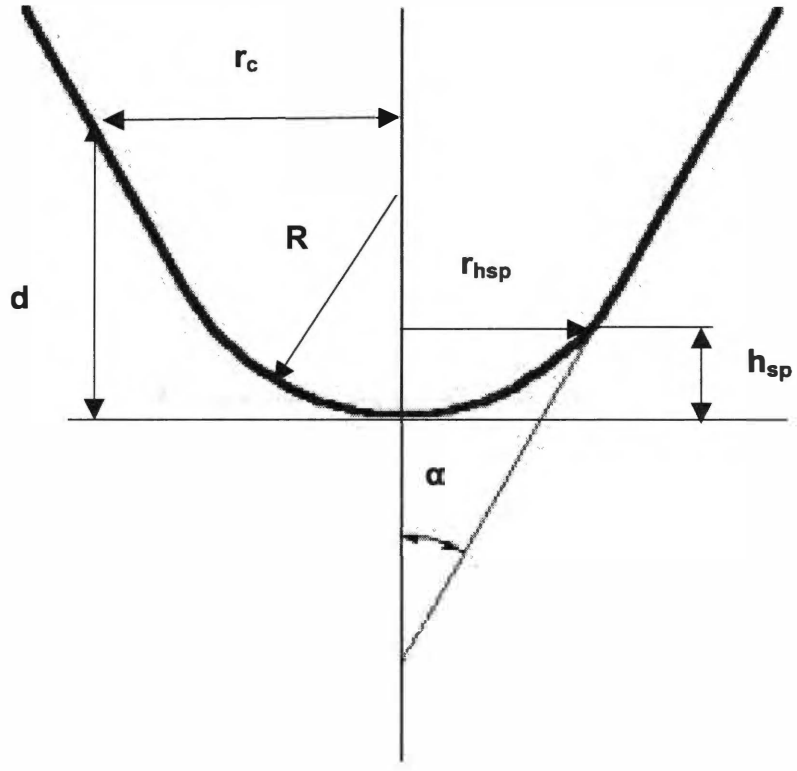


Figure 38: Parameters for description of the scratch tip geometry

At the height h_{sp}, the contact radius is r_{hsp} and can be found as:

$$r_{hsp} = \sqrt[2]{R^2 - (R - h_{sp})^2} \qquad \textbf{Equation 14}$$

More generally, at a given height **d**, the contact radius r_c can be expressed as:

If $d < h_{sp}$ $$r_c = \sqrt[2]{R^2 - (R - d)^2} \qquad \textbf{Equation 15}$$

If $d > h_{sp}$ $$r_c = r_{hsp} + (d - h_{sp}) \tan \alpha \qquad \textbf{Equation 16}$$

4.3.2 Strain rate

Figure 39 shows the influence of strain rate on the yield and fracture strengths σ_Y and σ_B, for PMMA [38]. An increase in the strain rate shifts the two curves up and to the right, which also means that the transition between the two behaviors is shifted to a higher temperature. This means that the PMMA becomes more brittle when the strain rate is increased.

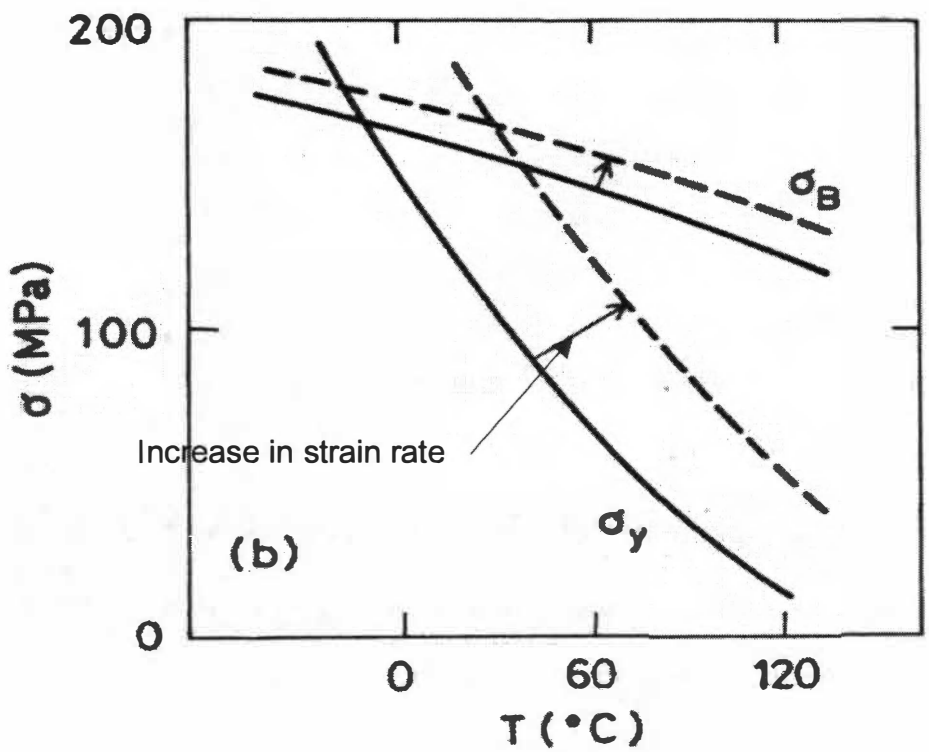


Figure 39: Effect of an increase in the strain rate on σ_B and σ_Y at temperature. The curves are shifted to the right and higher [38].

To compare these predictions with scratch test results requires a definition of the strain rate in the scratch test. The commonly accepted far field moderate rate [23, 24, 25, 39]:

$$\dot{\varepsilon}_S = \frac{Vtip}{a} \qquad \textbf{Equation 17}$$

will be used here.

4.3.2.1 Results for a 90° angle cone with a 2 µm tip radius

Experiments were performed at room temperature to examine the influence of the scratch strain rate on the critical load using first a 90° cone with a 2 µm tip radius. In order to obtain a variation in the scratch strain rate, the scratch speed was changed, giving scratch strain rate defined by **Equation 8.** The equivalence between scratch speed and strain rate is detailed in Table 3.

Figure 40 shows that the critical load decreases when the scratch strain rate is increased for the 90° cone. This means that the PMMA fractures at smaller loads when the strain rate, or the scratch speed, is increased.

Table 3: Scratch strain rates corresponding to the scratch speed

Speed	Strain rate
200 µm/s	15.0353 µm/µm/s
20 µm/s	1.2784 µm/µm/s
2 µm/s	0.1151 µm/µm/s
0.2 µm/s	0.0107 µm/µm/s

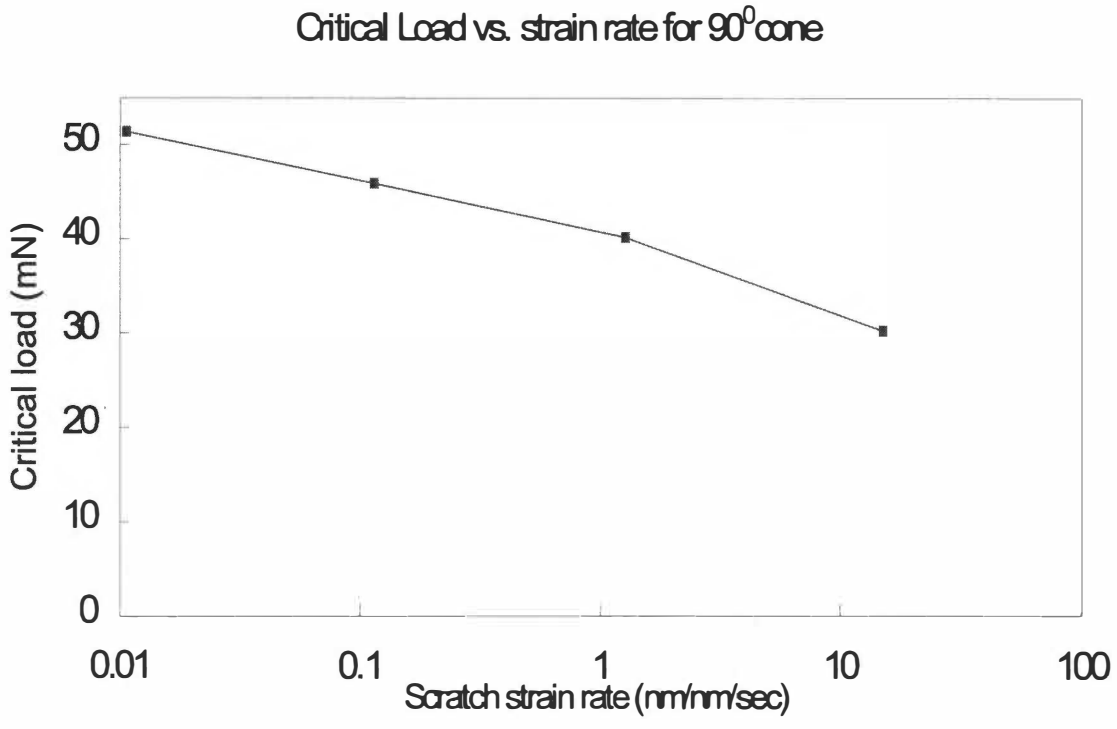


Figure 40: Critical load vs. scratch strain rate for a 90˚ cone with a 2µm radius

In Figure 41, the results are replotted on the graph of critical load vs. temperature. It is evident that increasing the strain rate has the same effect as decreasing the temperature, that is, it reduces the critical load and makes the material behave in a more brittle fashion. This confirms the effect of the strain rate shown on Figure 39.

4.3.2.2 Results for a 60° cone with a 4 μm tip radius

The strain rate dependence of the critical load for scratch experiments performed with a 60° angle cone with a 4 μm tip radius are shown in Figure 42. In this case the dependence of the critical load on strain rate is the opposite than the one seen for the 90° angle cone, that is the critical load increases with the strain rate rather than decreasing, which suggests that the PMMA is more brittle at smaller strain rates.

According to these experiments, the critical load, by itself, cannot be used reliably to predict the fracture behavior of a material as a function of the strain rate. One possible alternative is that fracture in PMMA occurs when a critical deformation is reached. This hypothesis is explored in the next section.

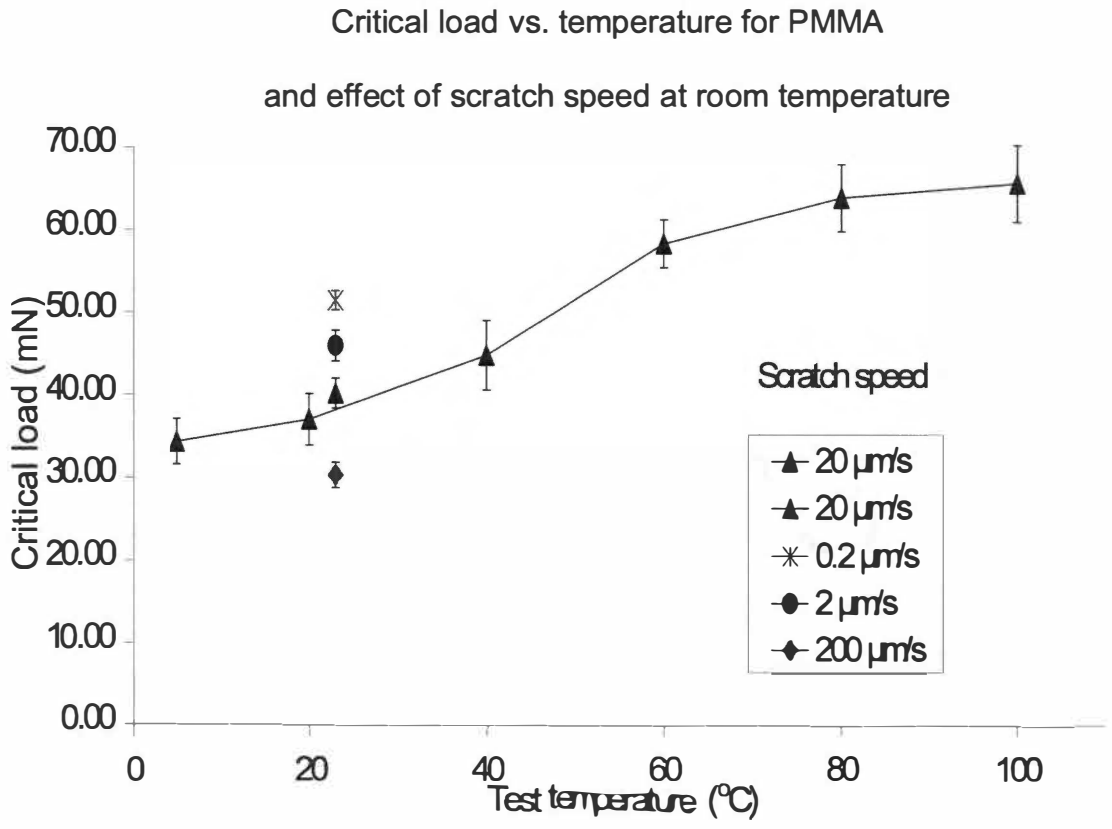


Figure 41: Critical load as function of temperature and effects of strain rate on the critical load at room temperature for scratch tests in PMMA using a 90˚ cone

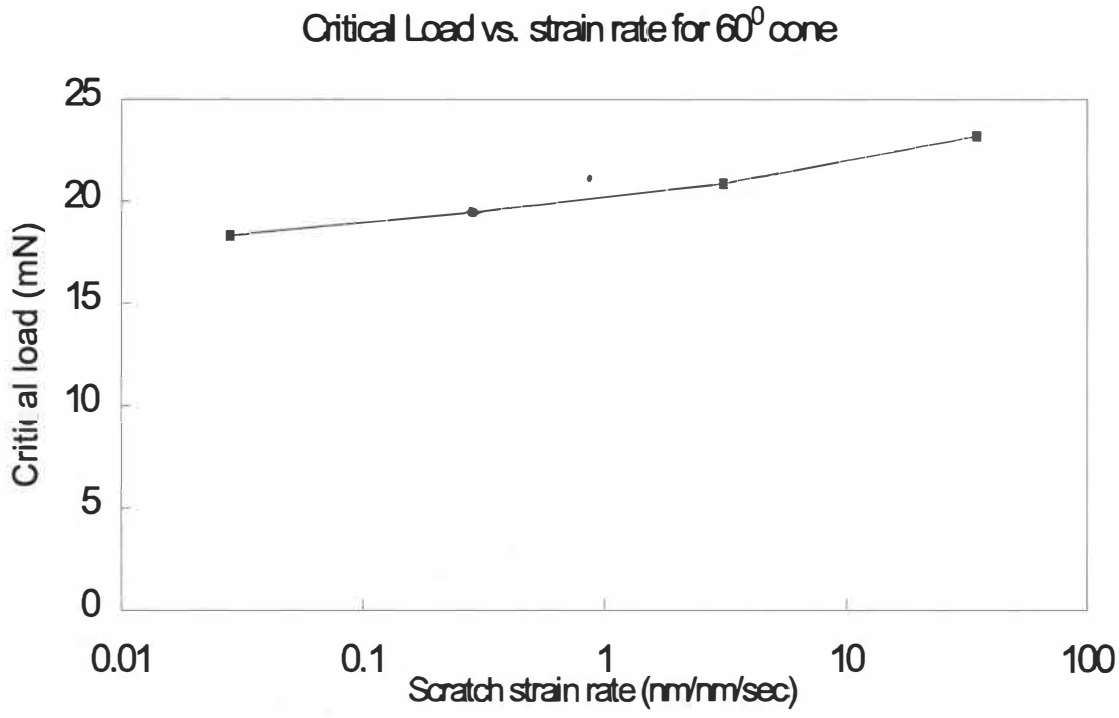


Figure 42: Critical load vs. scratch strain rate for 60˚ cone with a 4µm tip radius

4.3.3 Influences of deformation on fracture during scratching

In order to develop a better understanding of why the geometry of the scratch tip influences the fracture behavior, it is useful to examine the geometry of the scratch tip and how it influences the contact deformation in the material (Figure 19).

The scratch tip geometry can be divided into two main parts: that associated with the sphere at the tip, and the rest of the geometry, which is conical. These geometries impose a totally different degree of deformation and strain to the material during the scratch test. Tabor [1] had defined the equivalent strain for a sliding contact between a sphere and a plane as:

$$\varepsilon_s = 0.2\frac{r_c}{R}\frac{E}{\sigma_0} \qquad \textbf{Equation 18}$$

Where r_c is the contact radius, **R** is the sphere radius, **E** is the elastic modulus and σ_0 is the yield stress. This definition has been applied to scratch testing by other such as Gauthier [25] and Briscoe [40].

For the cone, the equivalent strain has been determined by K.L. Johnson [42] as:

$$\varepsilon_c = 0.2 \cot \alpha \frac{E}{\sigma_0} \qquad \textbf{Equation 19}$$

Where α is the half angle of the cone. However no one has studied the deformation of a cone with a rounded tip. If it is assumed that the total strain due to this scratch tip is a composite of the strains due to the two different geometries, one can develop a model that takes into account the effect of the two geometries. In this work, an exponential function has been chosen to fit and represent the total deformation ε_{Tot} of the blunted cone. Combining the effect of the two shapes, the approximation can be written as:

$$\varepsilon_{Tot} = \lambda\varepsilon_c(1 - e^{(-\theta r_c)}) + \gamma\varepsilon_s e^{(-\beta r_c)} \qquad \text{Equation 20}$$

Where, β, λ, γ, θ are fitting coefficients, and ε_s, ε_c are, respectively, the deformation due to a sphere and the deformation due to a cone. Equation 20 is a way to interpolate between the two different behaviors. The two limiting behaviors - the sphere deformation for small contact radii and to the cone deformation for larger contact radii - are the two asymptotes.

One has to keep in mind that this is a mathematical approximation of the combined effect of the deformation due to a sphere ε_s and the deformation due to a cone ε_c. This curve has no theoretical basis. This approximation is presented in Figure 43 for the 90° cone with 2μm radius. The two asymptotes represent the strain produced by a pure cone and a pure sphere. Note that the strain is caused by a cone is constant whatever the contact radius is. For the sphere, the strain increases with the contact radius. The exponential curve shows the approximation of the strain generated by the 90° cone with a 2 μm radius. Results of modeling the behavior by Equation 20 are presented in Figure 44 for both the 90° cone with a 2 μm tip radius and the 60° cone with a 4 μm tip radius. It is easy to see in the Figure 44 that for the same contact radius, the deformation caused by the two different scratch tips is significantly different. This observation suggests that it may be important to consider the depth at which the fracture occurs during scratching, as a function of the scratch speed. Results are shown in Table 4.

The table shows that for both scratch tips, the critical depth decreases as the scratch speed increases. Since the relationship between the contact radius r_c and the depth **d** (Figure 20), is known (**Equation 15** and **Equation 16**), the critical depth can be converted to a critical contact radius. Values of critical contact radius are shown as vertical lines on the plots Figure 45 and Figure 46,

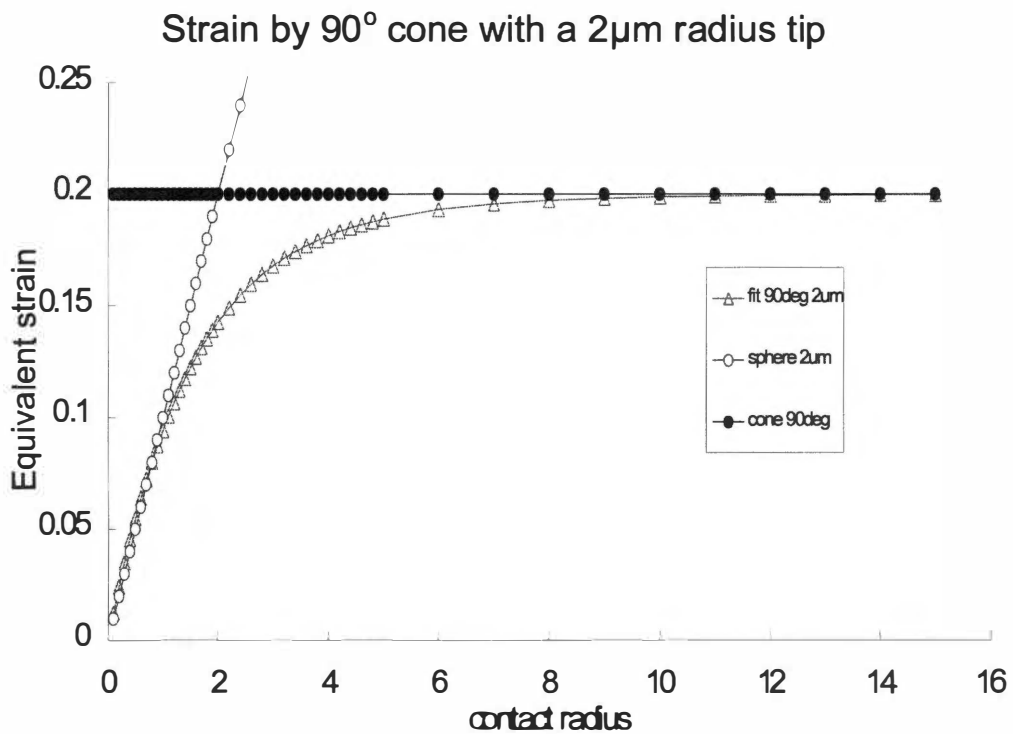


Figure 43: Equivalent strain generated by a 90° cone with a tip radius of 2µm

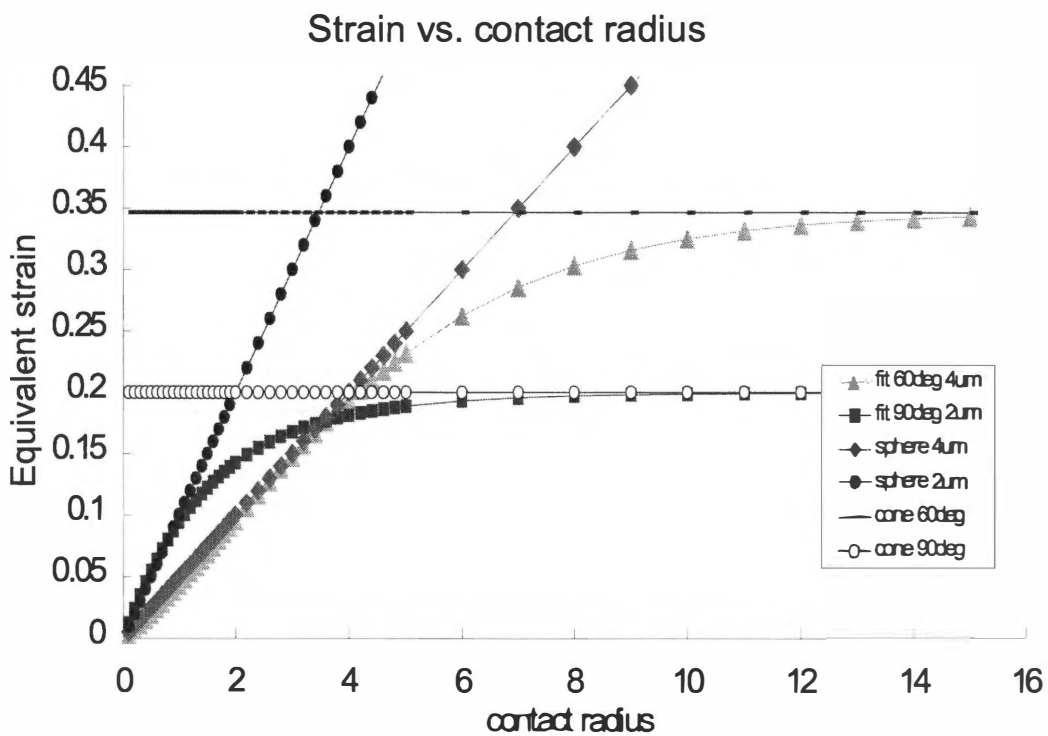


Figure 44: Equivalent strain vs. contact radius for the two different scratch tips: a 60˚cone with a 4µm radius and a 90˚ cone with a 2µm radius

Table 4: Critical depth vs. scratch speed for thye two different scratch tips

	0.2 µm/s	2 µm/s	20 µm/s	200 µm/s
90˚ cone 2µm radius	7.083 µm	6.155 µm	5.177 µm	4.076 µm
60˚ cone 4µm radius	4.082 µm	3.929 µm	3.801 µm	3.784 µm

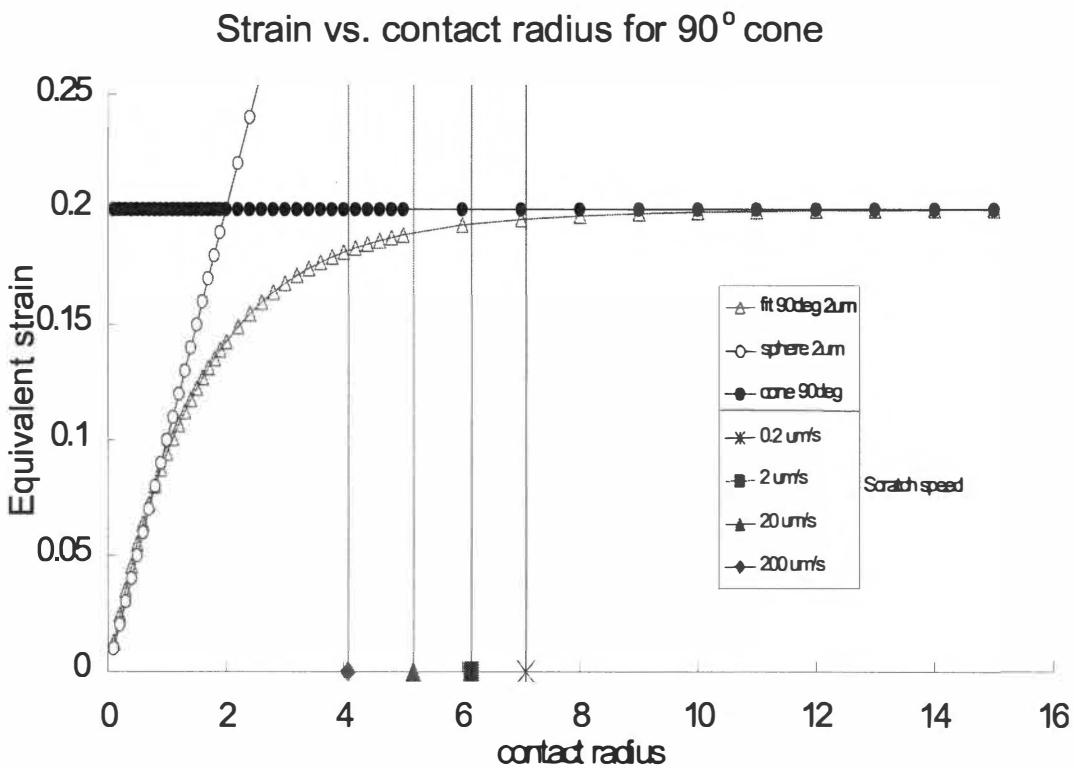


Figure 45: Contact radii at fracture for different scratch speeds demonstrating the equivalent strain at fracture for the 90˚ cone

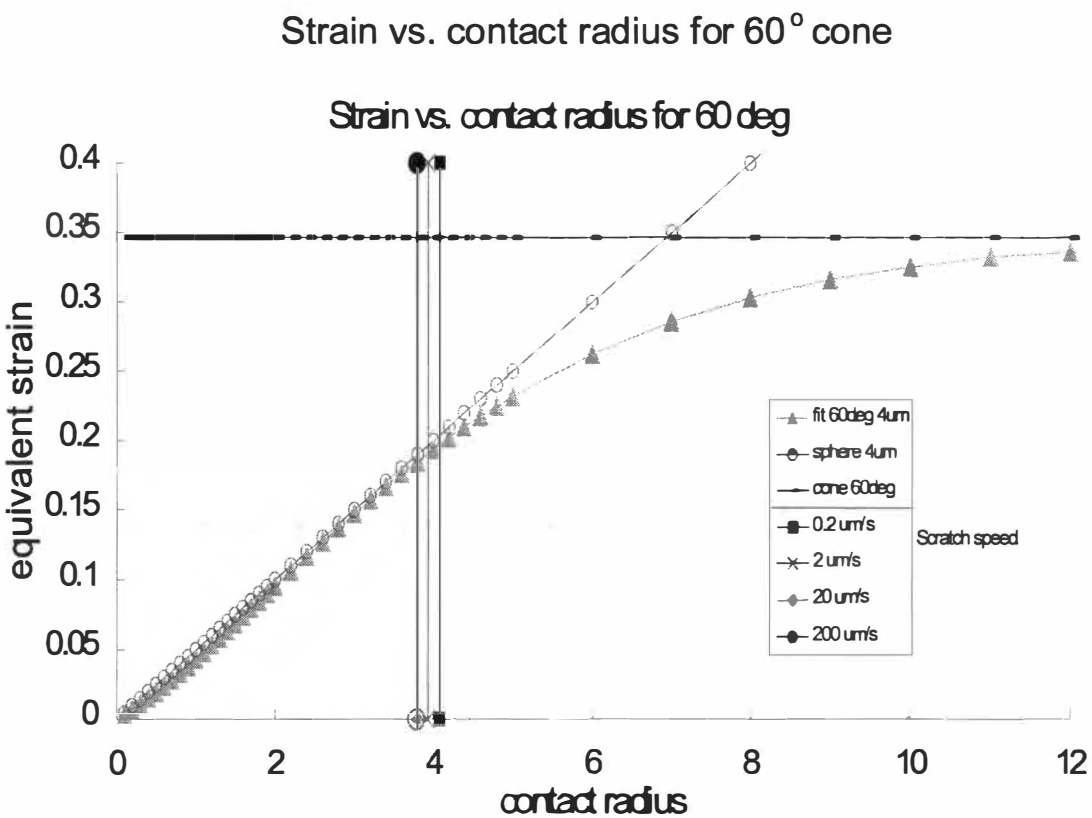


Figure 46: Contact radii at fracture for different scratch speeds demonstrating the equivalent strain at fracture for the 60˚ cone

which estimate the deformation, caused by the scratch tip. On these plots, the four different scratch speeds generate four different critical contact radii for each tip. The intersection between these vertical lines and the approximation of the deformation, due to the scratch tip, gives the deformation at fracture.

For the case of the 90° cone (Figure 45), it is interesting to note that fracture occurs at a depth that is into the conical part of the scratch tip. The deformation at fracture is thus more due to a cone than to a sphere. Moreover this is true for all the scratch speeds.

For the 60° cone (Figure 46), fractures occur in the spherical part of the scratch tip well before the transition to the cone. Note that the different scratch speeds generate fracture over a smaller range of strain than for the 90° cone. This is due to the fact that the strain increases rapidly as a function of contact radius for the sphere but stays constant for the cone.

The two plots in Figure 45 and Figure 46, presenting an approximation of the deformation due to the scratch tip as a function of the contact radius can be used to determine the strain at the fracture point for the different scratch speeds. Results are presented in Table 5 and Table 6.

Table 5: Critical values for the 60° cone

Speed µm/s	Critical load mN	Critical depth µm	Critical contact radius µm	Equivalent strain at fracture µm / µm	Critical strain rate µm / µm /s
0.2	18.362	3.070	4.082	1969.94E-4	0.049
2	19.493	2.806	3.929	1905.23E-4	0.508
20	20.903	2.584	3.801	1849.43E-4	5.261
200	23.223	2.555	3.784	1842.06E-4	52.845

Table 6: Critical values for the 90° cone

Speed µm/s	Critical load mN	Critical depth µm	Critical contact radius µm	Equivalent strain at fracture µm/ µm	Critical strain rate µm / µm/s
0.2	51.4	6.255	7.083	1958.71E-4	0.028
2	45.906	5.326	6.154	1936.81E-3	0.325
20	40.16	4.348	5.177	1898.80E-4	3.863
200	30.30	3.247	4.075	1822.16E-4	49.068

Knowing the critical contact radius and the scratch speed, one can calculate the "critical strain rate", at which the fracture occurs as follows:

$$\dot{\varepsilon}_{critical} = \frac{V_{tip}}{r_{c_{critical}}} \qquad \textbf{Equation 21}$$

Results for the critical strain rate are also presented in Table 5 and Table 6.

Using the results in Table 5 and Table 6 Figure 47 shows a plot of the critical deformation vs. critical strain rate. For both scratch tips the two curves are very similar and exhibits the same trends. In order to compare the two curves they have been fitted with a log function (Figure 47). The two curve fits return very similar equations:

For the 60° cone:

$$y = -0.0018\text{Ln}(x) + 0.1907$$

For the 90° cone

$$y = -0.0019\text{Ln}(x) + 0.1901$$

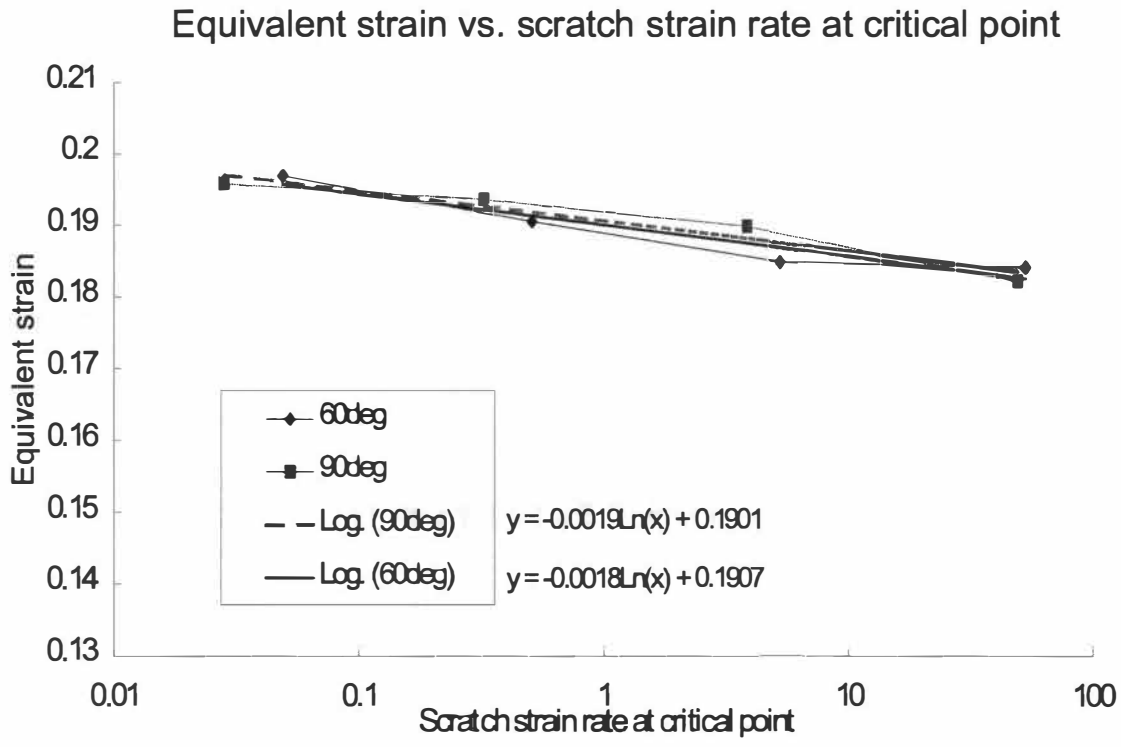


Figure 47: Equivalent strain vs. critical strain rate for the two scratch tips and their respective fits

It is interesting to note that these results do not depend upon the tip geometry and can therefore be considered as material properties much in the same manner as the hardness or the modulus.

Furthermore, the data in Figure 42 help to explain the contradiction that was noticed in the critical load evolution as function of the strain rate (Figure 40 and Figure 42). These plots have to be considered differently in order to explain the contradiction in behavior of the two scratch tips. The curves critical load as a function of the strain rate must be viewed as a curve limit above which the material fractures. As shown in Figure 48, if a given load applied at a given strain rate is represented on the plot by a point, the material will fracture if the point is above the limit curve and won't fracture if the point is below the limit curve. If the material fractures at a given strain rate and a given load (point on the limit curve), an increase of the strain rate keeps the material in "fracturing mode", in the case of the 90° cone, and causes the fracture stop in the case of the 60° cone (arrows in Figure 48).

The same reasoning can be applied on the plot of equivalent strain vs. strain rate at fracture (Figure 47); crossing the fitted line, from left to right, causes the material to fracture. The difference in the plot of Figure 47 is that deformation and strain rate are changing at the same time.

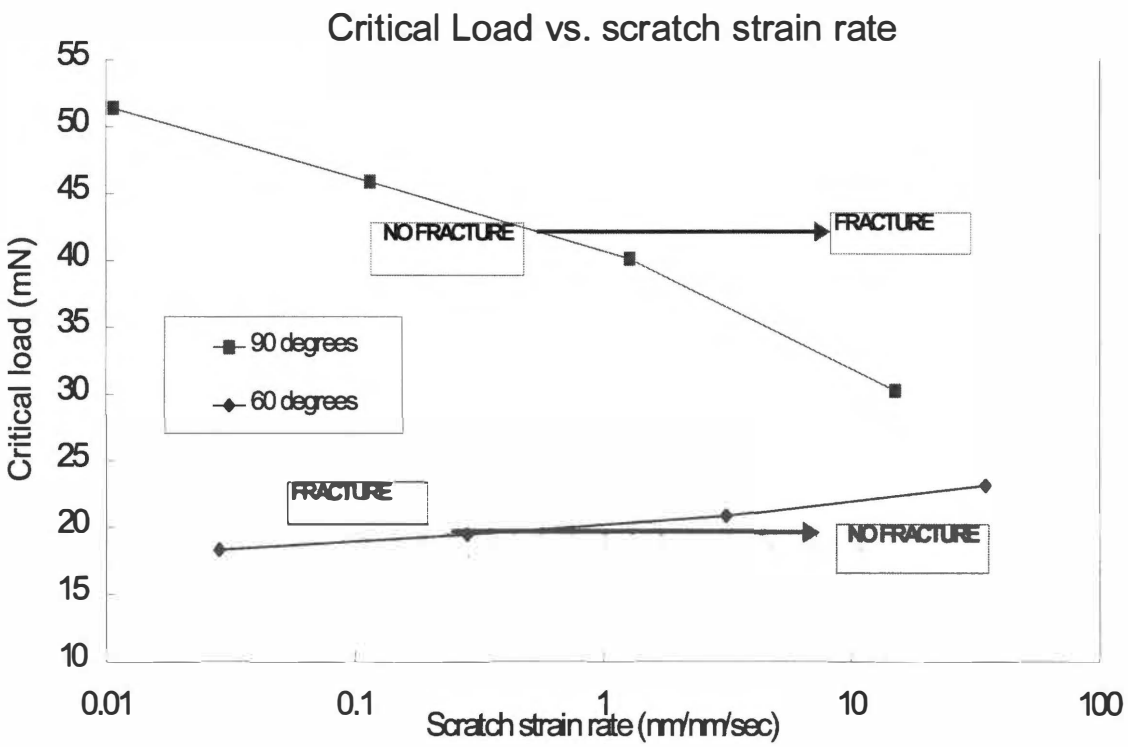


Figure 48: Critical load vs. scratch strain rate defining the limits of the domain of fracture

Thus, the increase in strain rate at a constant load is not a horizontal line because the equivalent strain at fracture changes with the strain rate.
According to the strain rate definition given in **Equation 8**, an increase in strain rate means a decrease in contact radius.

Figure 45 and Figure 46 show that the same variation in contact radius generates a larger change in equivalent strain for the 60° cone than for the 90° cone. In the case of the 90° cone, the change in strain is small. These observations can be understood from Figure 47, where an increase in strain rate for the 90° cone produces a small change in strain and keeps the material in the "fracture zone" above the curve limit. For the 60° cone, an increase in strain rate decreases the strain more dramatically. Therefore, the strain caused by the 60° cone becomes smaller than the critical strain and subsequently, the material stops fracturing (Figure 49).

4.3.4 Use of the results in scratch analysis

The new results can be used to characterize an unknown material or to predict when the fracture during scratching will occur for a given material for which some properties are known.

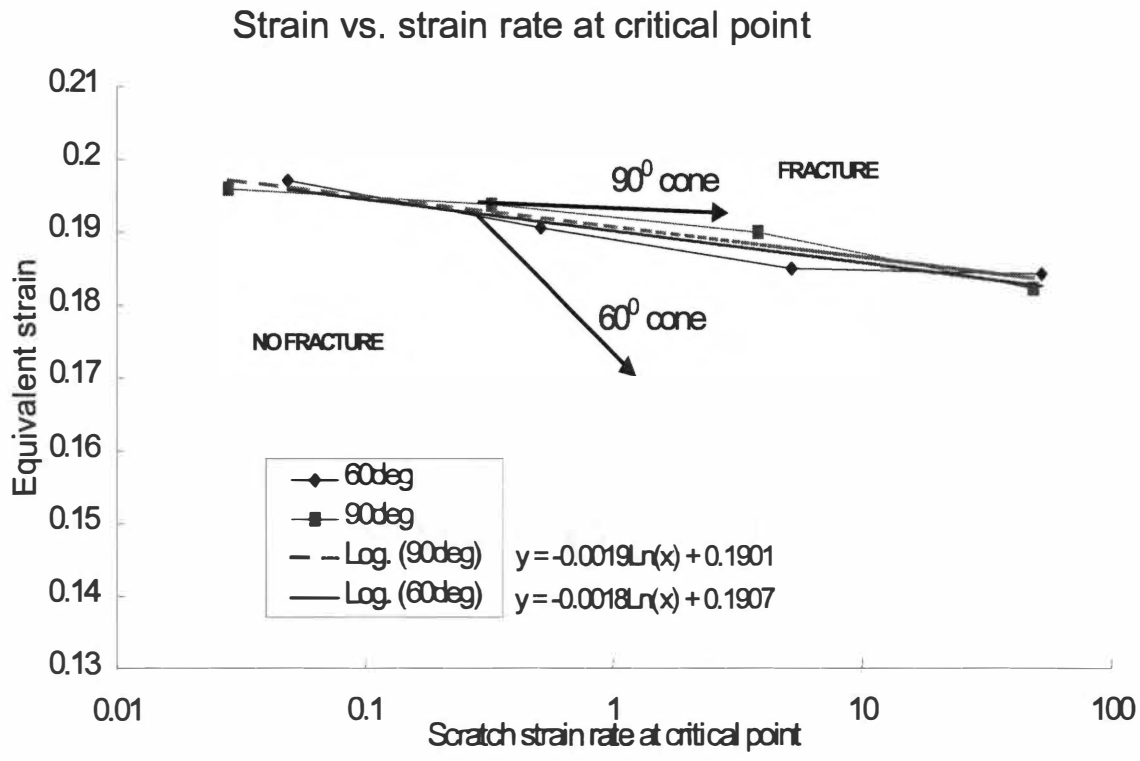


Figure 49: Effect of an increase in the strain rate on the fracture process for the two different scratch tips.

4.3.4.1 Unknown Material

In this case the indenter geometry is given and scratches are made on the material at different speeds. Each test gives a critical load and critical depth. **Equation 15** or **Equation 16** allows the calculation of the critical contact radius from the critical depth. Then, the critical contact radius is used to determine the critical strain rate by means of **Equation 21**, and the critical strain via the approximation of the deformation due to the indenter represented by **Equation 20**. This process is illustrated in Figure 50.

The dependence of the critical strain on the critical strain rate can be plotted in the manner of Figure 47, which can be considered as a material behavior. Another material behavior that can be obtained is the dependence of the contact pressure, or scratch hardness, on the scratch strain rate (Figure 51).

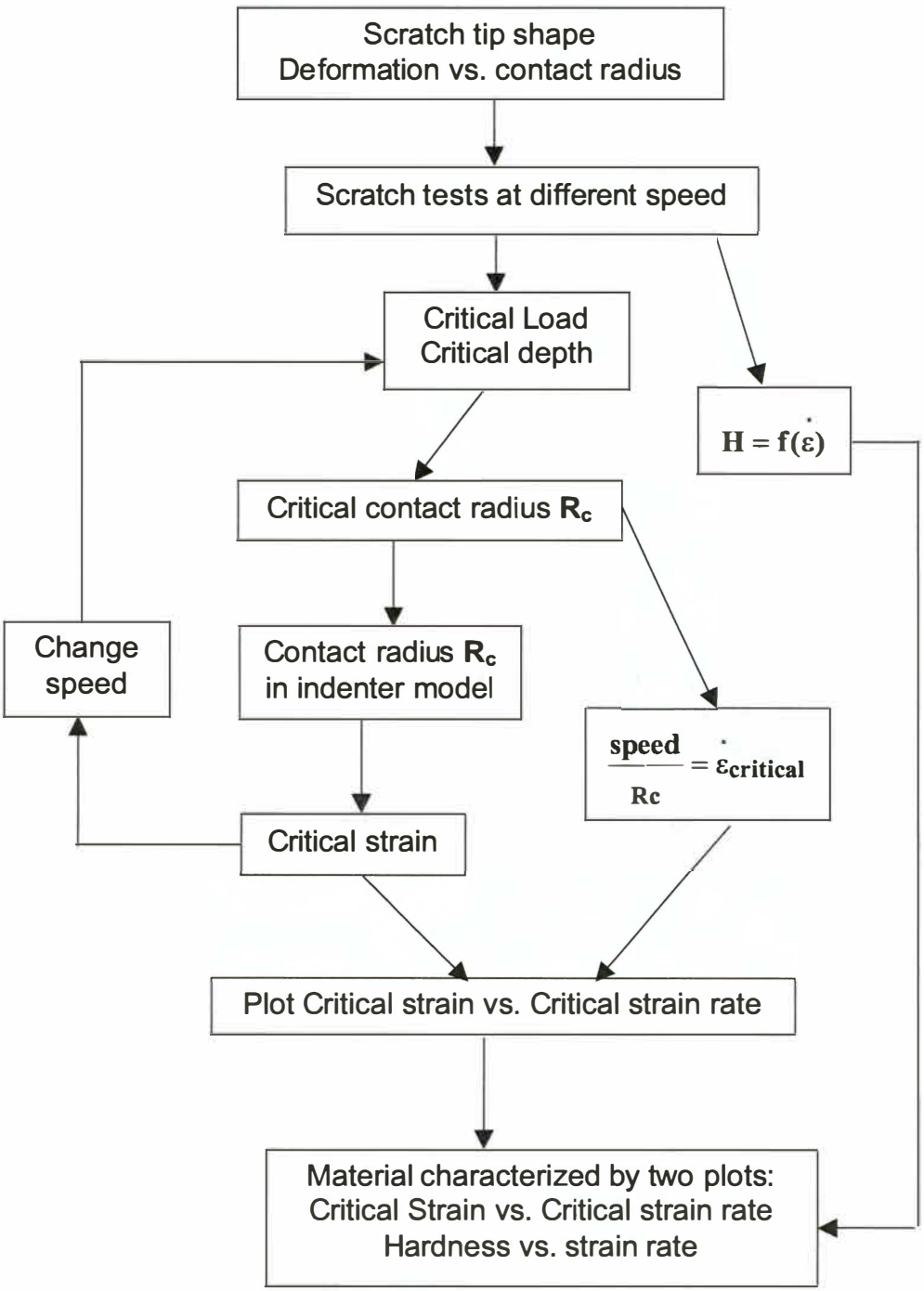


Figure 50: Process for determining the critical properties of an unknown material by scratch testing

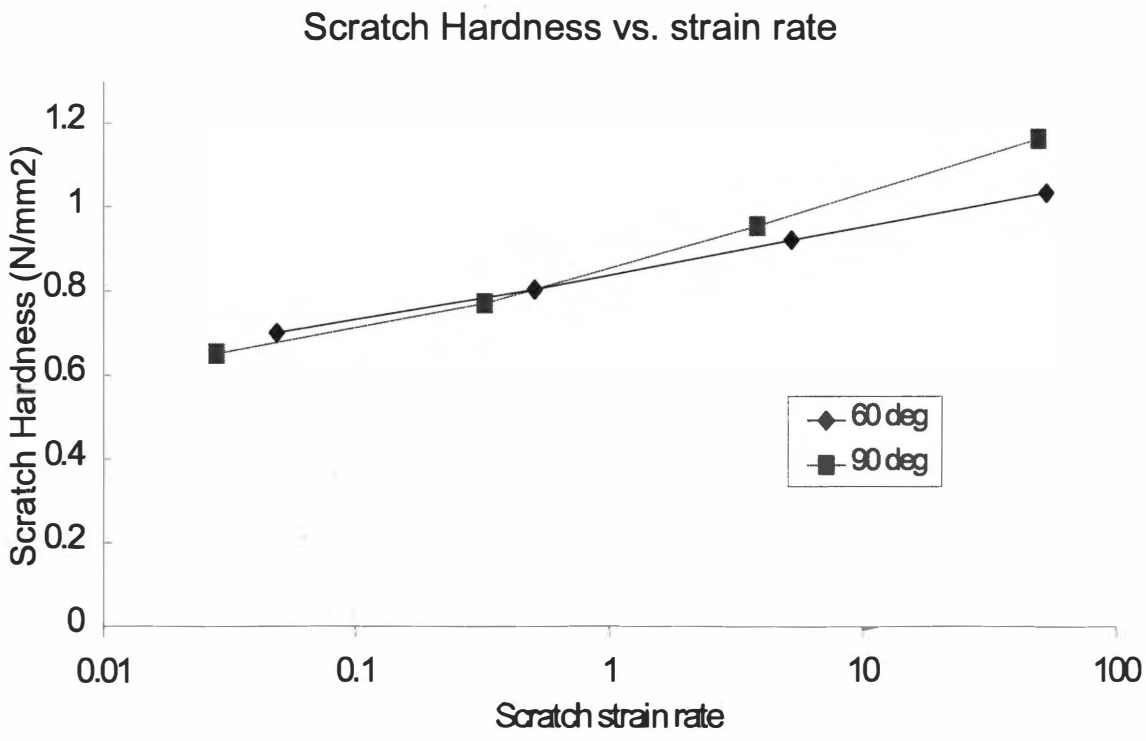


Figure 51: Dependence of scratch hardness on strain rate for PMMA

4.3.4.2 *Material with a known scratch behavior*

In this case, plots of scratch hardness vs. strain rate, $\mathbf{H_s=f(\dot{\varepsilon})}$ (Figure 51), and, critical strain vs. critical strain rate (Figure 47), are known for the material. The geometry of the scratch tip is also known.

From the scratch tip geometry and the plot $\mathbf{H_s=f(\dot{\varepsilon})}$, the contact radius can be calculated at each point as a function of the strain rate and then, as a function of the scratch speed. The contact radius can be plotted on a graph of equivalent strain vs. contact radius (Figure 44), which is obtained from the indenter geometry. The equivalent strain can be extracted from this last graph and plotted as a function of scratch speed. With known values for the contact radius, the equivalent strain and the scratch speed, one can plot a curve showing the dependence of the deformation on the strain rate. Then, the intersection between critical strain vs. critical strain rate and strain vs. strain rate gives the point of fracture. This process is illustrated in Figure 52.

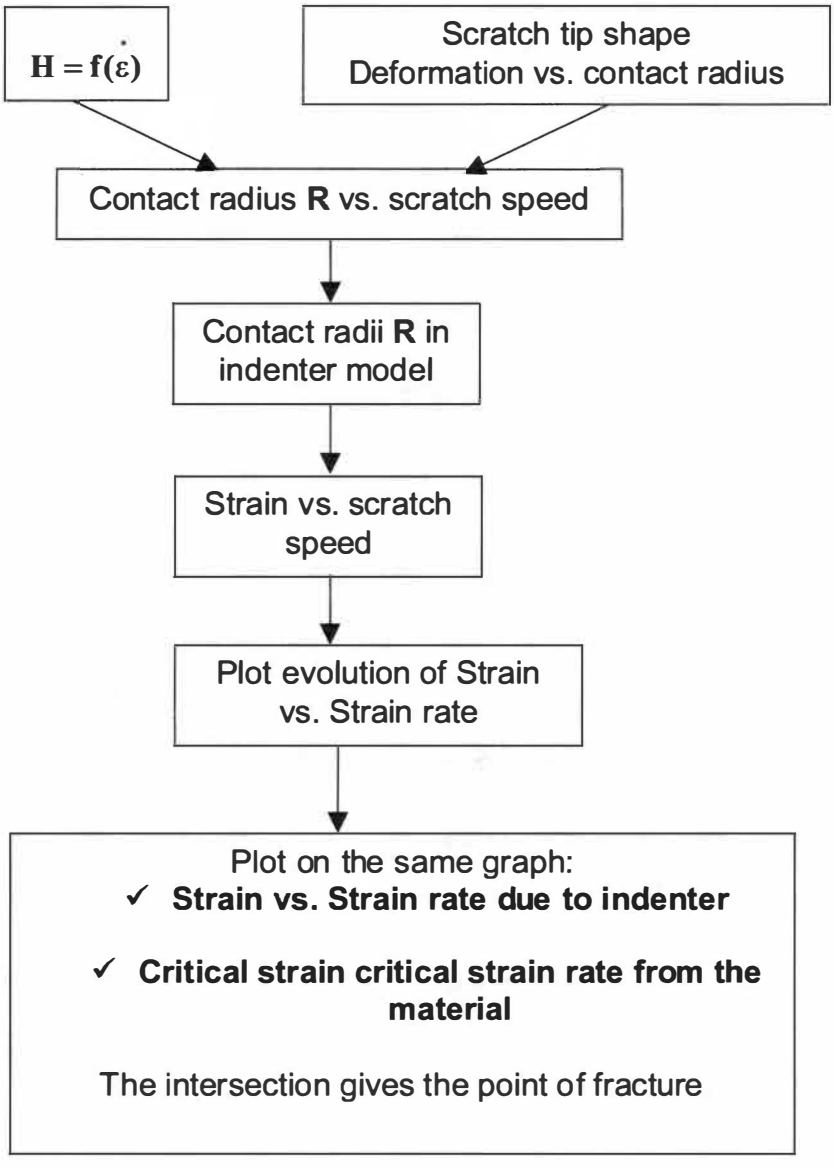


Figure 52: Process for predicting the point of fracture by scratching test on a known material

CHAPTER 5: CONCLUSIONS

In the first part of the study, the temperature was used to relate the mechanical properties of PMMA measured by indentation and scratch testing. One important result is the equivalence between the indentation hardness and the scratch hardness.

Cross sectional profiles of scratch tracks allowed an analysis of the plastic deformation produced in a scratch. The pile-up height shows a strong correlation with the ratio **E/H**. This correlation has been shown for different temperatures and strain rates

Influences of temperature were used to study the critical load at fracture during scratch testing. From experiments conducted at several temperatures along with data from the literature, a hypothesis was formulated concerning the origin of fracture during scratch testing. According to the hypothesis, fracture is generated by tensile stresses that develop behind the scratch tip.

With an approximation of the strain produced in the material due to the scratch tip and the results obtained from scratch tests at different strain rates, the

deformation strain was revealed as a very important parameter in the origin of fracture during scratching of PMMA. The influence of the geometry of the scratch tip can be separated by considering the equivalent strain for fracture. A plot of critical strain vs. critical strain rate can be used to characterize the important material properties. The results of this work can be applied to predict when fracture will occur in other material with other scratch tips.

CHAPTER 6: SUGGESTIONS FOR FUTURE RESEARCH WORK

In order for this work to be complete, more experiments with different tip radii are necessary.

What has been presented as an approximation of the equivalent strain, due to the scratch tip could be calculated by finite elements simulation to provide a more precise estimation of this deformation.

Instead of using the literature data, tensile test data obtained on exactly the same material used for scratch testing would be useful for the purpose of developing models.

Further experiments can be conducted recording the lateral forces, to have a better understanding of the influence of the friction between the indenter and the surface.

Experiments could be conducted on materials other than the PMMA to verify that the hypotheses presented in this work are valid.

BIBLIOGRAPHY

BIBLIOGRAPHY

1 - D.S. Tabor, *Hardness of Metals* (Clarendon Press, Oxford, 1951)

2 - P. J. Blau, *Fifty years of research on the wear of metals*, Tribology International Vol. 30 No. 5, **239**, (1997).

3 - P.R. Chalker, S.J. Bull and D.S. Rickerby, *A review of the methods for the evaluation of coating-substrate adhesion*, Materials Science and Engineering, A140 (1991)

4 - K. Adamsons, R.J. Barsotti, L. Lin, B.V. Gregorovich, P. McGonigal, B. Neff, G.S. Blackman, D. Nordstrom, J. Johnson, *Scratch and mar testing: general issues and application of the single nano-indenter micro-scratch technique in study of newly prepared and aged clearcoats*, ACS meeting, Boston, (1994).

5 - G.S. Blackman, L.Lin, R.R. Matheson, *Micro and nano wear of polymeric materials*, Polymer preprints, Vol.39, No 2, **1218-1219** (1998).

6 - U. Biskup, *Optimizing the scratch resistance of pur automotive clear coats*, 4th Nürnberg Congress, Paper 57, (1997)

7 - T.A. Potter, P.B. Jacobs, T. Engbert, M. Bock, *Scratching of automotive OEM clear coats method and media effects*, SAE International, Detroit, 980975 (1998)

8 - R.A. Ryntz, B.D. Abell, F. Hermosillo, *Scratch resistance of automotive plastic coatings*, SAE International, Detroit, 980973 (1998)

9 - L. Lin, G.S. Blackman, R.R. Matheson, *Micro-mechanical characterization of scratch and mar behavior of automotive topcoats*, ACS meeting, Boston (1994).

10 - A.C. Ramamurthy, J.A. Charest, M.D. Lilly, D.J. Mihora, J.W. Freese, *Friction induced paint damage – a novel method for objective assessment of painted engineering plastics*, Wear, 203-204, **350-361**, (1997)

11 - P.B. Jacobs, T. Engbert, *Studies on scratch and mar resistance of polyurethane coatings*, SAE International, Detroit, 960913, (1996)

12 - R.I. Trezona, I.M. Hutchings, A.C. Ramamurthy, *A new technique for determining the micro-scale abrasion resistance of automotive clear coats*, Automotive Automation Limited, 97PA018, **913-919**, (1997)

13 - W. Shen, C. Ji, F. Jones, M.P. Everson, A Ryntz, *Measurement by scanning force microscopy of the scratch and mar resistance of surface coatings*, Surface Coatings International, **253-256**, (1996)

14 - G.D. Cheever, R.A. Ottaviani, V.R. Iyengar, *Use of the goniophotometer for scratch and mar testing of automotive top coats*, SAE Technical Paper Series, 970998, (1997)

15 - A.C. Ramamurthy, D.J. Mihora, *Durability of painted automotive exteriors: a study in paint Tribology*, Automotive Automation Limited, **905-912**, (1997)

16 - C. Xiang, H.J. Sue, J. Chu, B. Coleman, *Scratch behavior and material property relationship in polymers*, Journal of polymers science, Vol. 39, **47-59**, (2001)

17 - V. Jardret, B.N. Lucas, W.C. Oliver, *Scratch durability of automotive clear coatings: a quantitative, reliable and robust methodology*, Journal of coatings technology, Vol. 72, **79-88** (2000)

18 - V.D. Jardret, W.C. Oliver, *Viscoelastic behavior of polymer films during scratch test: a quantitative analysis*, Mat. Res. Soc. Symp. Proc., 594, **251-256**, (2000)

19 - B. Lamy, T. Mathia, *Formation of wear fragments by fracture processes in abrasive contacts*,

20 - B.J. Briscoe, P.D. Evans, E. Pelillo, S.K. Sinha, *Scratching maps for polymers*, Wear, 200, **137-147**, (1996)

21 - B.J. Briscoe, *Isolated contact stress deformations of polymers; the basis for interpreting polymer Tribology*, Mechanical Eng. Publications Ltd., **191-196**, (1997)

22 - A.G. Atkins, *Fracture toughness and cutting*, Int. J. Prod. Res., Vol. 12, **263-274**, (1974)

23 - C. Gauthier, R. Schirrer, *Time and temperature dependence of the scratch properties of poly(Methylmethacrylate) surfaces*, Journal of Materials Science, Vol. 35, No 9, **2121-2130**, (2000)

24 - C. Gauthier, R. Schirrer, *The viscoelastic viscoplastic behavior of a scratch on a polymeric surface*, EUROMAT 2000 Conference on Advances in Mechanical Behaviour Plasticity and Damage, Tours, (2000)

25 - C. Gauthier, S. Lafaye, R. Schirrer, *Elastic recovery of a scratch in a polymeric surface: experiments and analysis*, Tribology International, **1-11**, (2001)

26 - Y.Xie, H.M. Hawthorne, *A controlled scratch test for measuring the elastic property, yield stress and contact stress-strain relationship of a surface*, Surface Coating Technology, 127, **130-137**, (2000)

27 - B.R. Lawn, S.M. Wiederhorn, D.E. Roberts, *Effect of sliding friction forces on the strength of brittle materials*, Journal of materials science, 19, **2561-2569**, (1984)

28 - U. Schulz, V. Wachtendorf, T. Klimmasch, P. Alers, *The influence of weathering on scratches and on scratch and mar resistance of automotive coatings*, Progress in organic coatings, 42, **38-48**, (2001)

29 - T. Meschievitz, Y. Rahangdale, R. Pearson, *A unique approach to powder painting technology development*, USCAR low emission paint Consortium, October 1995

30 - N.X. Randall, G. Favaro, C.H. Frankel, *The effect of intrinsic parameters on the critical load as measured with the scratch test method*, Surface and coatings technology, 137, **146-151**, (2001)

31 - V.D. Jardret, H. Zahouani, J.L. Loubet, T.G. Mathia, *Understanding and quantification of elastic and plastic deformation during a scratch test*, Wear, 218, **8-14**, (1998)

32 - M.F. Doerner, W.D. Nix, J. Mater Res, **1**, 601, (1986)

33 - W.C. Oliver, G.M. Pharr, J. Mater Res, **7**, 1564, (1992)

34 - H.E. Hintermann, *Characterization of surface coatings by the scratch adhesion test and by indentation measurements*, Fresenius J Anal Chem, 346, **45-53**, (1993)

35 - G.M. Pharr, W.C. Oliver, F.R. Brotzen, J. mater. Res., 7, 613, (1992)

36 - B.N. Lucas, *An experimental investigation of creep and viscoelastic properties using depth-sensing indentation techniques*, Ph. D. Dissertation, University of Tennessee, Knoxville, (1997)

37 - V.D. Jardret, W.C. Oliver, *On the robustness of scratch testing for thin films: the issue of tip geometry for critical load measurement*, Materials Research Society Symp., Vol. 594, **394-400**, (2000)

38 - E. Riande, R. Diaz-Calleja, M.G. Prolongo, R.M. Masegosa, C. Salom, *Polymer Viscoelasticity*, (Marcel Dekker., New york, Basel, 2000) **614-615**

39 - B.J. Briscoe, P.S. Thomas, Tribology transactions, 38, **382**, (1995)

40 - B.J. Briscoe, Tribol. Int., 31 (1-3): 121, (1998)

41 - F.P. Bowden, D. Tabor, *The friction and lubrification of solids* (Clarendon press, Oxford, Part1, 1950, part 2 1964)

42 - K.L. Johnson, *Contact Mechanics*, (Cambridge University Press, Cambridge, 1985)

43 - B.N. Lucas, W.C. Oliver, J.E. Swindeman, Proc. Mat Res. Soc. Symp., 436, 1998.

44 - J-L. Loubet, B.N. Lucas, W.C. Oliver, NIST Special Publication 896 – *Conference Proceedings: International Workshop on Instrumented Indentation*, Eds. D.T. Smith (NIST 1995) pp. 31-34

VITA

Pierre Jean Morel was born January 3, 1977 in Tassin la Demi Lune, FRANCE. He attended intermediate school at the "Aux Lazaristes" school in Lyon, France. He obtained, in 1994, his Baccalauréat C with a math major, after his high school in "Lycée du Sacré Cœur" in Tournon, France. Then, in 1995, he obtained with distinctions, a Baccalauréat S, with technology and math option. Then, between 1995 and 2000, he studied in "Ecole d'Ingénieurs de Saint Etienne" (E.N.I.S.E) at St Etienne, France, from which he graduated in May 2000,obtaining a mechanical engineer diploma. During his last year at the E.N.I.S.E, he did an internship at MTS Nano Instruments Innovation Center, in Oak Ridge, Tennessee. From there, he entered graduate school at the University of Tennessee in Knoxville in 2000. While enrolled at the University of Tennessee, his research was performed at the MTS Nano Instruments Innovation Center, and supervised by Dr. George Pharr, Professor of the Materials Science and Engineering Department in the University of Tennessee. His Masters degree was conferred in May 2002.

3784 2850 24
08-07-02 MAB